

1 **Cluster Dynamics-based Parameterization for Sulfuric Acid-Dimethylamine**
2 **Nucleation: Comparison and Selection through Box- and Three-Dimensional-**
3 **Modeling**

4 Jiewen Shen^{1,2}, Bin Zhao^{1,2}, Shuxiao Wang^{1,2,*}, An Ning³, Yuyang Li², Runlong Cai⁴,
5 Da Gao^{1,2}, Biwu Chu^{5,6}, Yang Gao⁷, Manish Shrivastava⁸, Jingkun Jiang², Xiuhui
6 Zhang³, Hong He^{5,6}

7
8 ¹*State Key Joint Laboratory of Environment Simulation and Pollution Control, School*
9 *of Environment, Tsinghua University, Beijing, 100084, China*

10 ²*State Environmental Protection Key Laboratory of Sources and Control of Air*
11 *Pollution Complex, Beijing, 100084, China*

12 ³*Key Laboratory of Cluster Science, Ministry of Education of China, School of*
13 *Chemistry and Chemical Engineering, Beijing Institute of Technology, Beijing, 100081,*
14 *China*

15 ⁴*Shanghai Key Laboratory of Atmospheric Particle Pollution and Prevention (LAP³),*
16 *Department of Environmental Science & Engineering, Fudan University, Shanghai,*
17 *200438, China*

18 ⁵*State Key Joint Laboratory of Environment Simulation and Pollution Control,*
19 *Research Center for Eco-Environmental Sciences, Chinese Academy of Sciences,*
20 *Beijing 100085, China*

21 ⁶*College of Resources and Environment, University of Chinese Academy of Sciences,*
22 *Beijing 100049, China*

23 ⁷*Key Laboratory of Marine Environment and Ecology, Ministry of Education, Ocean*
24 *University of China, Qingdao 266100, China*

25 ⁸*Pacific Northwest National Laboratory, Richland, Washington, USA*

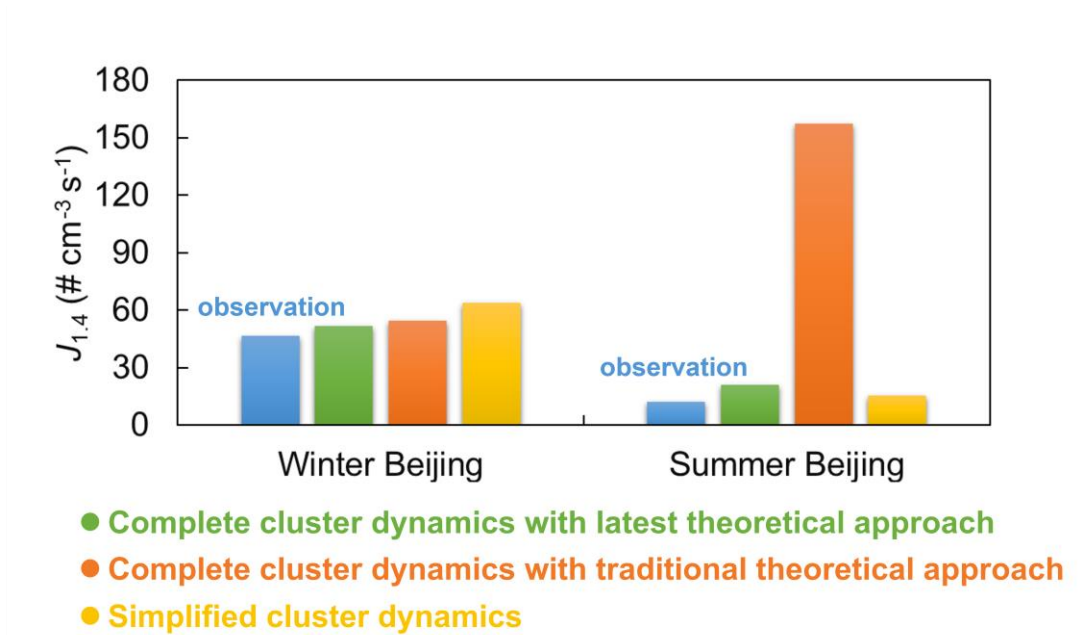
26

27 *Correspondence to: Shuxiao Wang (shxwang@tsinghua.edu.cn)

28 **ABSTRACT**

29 Clustering of gaseous sulfuric acid (SA) enhanced by dimethylamine (DMA) is a
30 major mechanism for new particle formation (NPF) in polluted atmospheres. However,
31 uncertainty remains regarding the SA-DMA nucleation parameterization that
32 reasonably represents cluster dynamics and is applicable across various atmospheric
33 conditions. This uncertainty hinders accurate three-dimensional (3-D) modeling of NPF
34 and subsequent assessment of its environmental and climatic impacts. Here we
35 extensively compare different cluster dynamics-based parameterizations for SA-DMA
36 nucleation and identify the most reliable one through a combination of box-model
37 simulations, 3-D modeling, and in-situ observations. Results show that the
38 parameterization derived from Atmospheric Cluster Dynamic Code (ACDC)
39 simulations, incorporating the latest theoretical insights (DLPNO-CCSD(T)/aug-cc-
40 pVTZ// ω B97X-D/6-311++G(3df,3pd) level of theory) and adequate representation of
41 cluster dynamics, exhibits dependable performance in 3-D NPF simulation for both
42 winter and summer conditions in Beijing and shows promise for application in diverse
43 atmospheric conditions. Another ACDC-derived parameterization, replacing the level
44 of theory with RI-CC2/aug-cc-pV(T+d)Z//M06-2X/6-311++G(3df,3pd), also performs
45 well in NPF modeling at relatively low temperatures around 280 K but exhibits
46 limitations at higher temperatures due to inappropriate representation of SA-DMA
47 cluster thermodynamics. Additionally, a previously reported parameterization
48 incorporating simplifications is applicable for simulating NPF in polluted atmospheres
49 but tends to overestimate particle formation rates under conditions of elevated
50 temperature ($> \sim 300$ K) and low condensation sink ($< \sim 3 \times 10^{-3} \text{ s}^{-1}$). Our findings
51 highlight the applicability of the new ACDC-derived parameterization, which couples
52 the latest SA-DMA nucleation theory and holistic cluster dynamics, in 3-D NPF
53 modeling. The ACDC-derived parameterization framework provides valuable reference
54 for developing parameterizations for other nucleation systems.

55 **GRAPHICAL ABSTRACT**



56

57 1 INTRODUCTION

58 Atmospheric aerosols have significant impacts on visibility, human health, and
59 global climate (Gordon et al., 2016; Gao et al., 2024). New Particle Formation (NPF)
60 is the predominant source of global aerosol population, with nucleation being the key
61 stage of the gas-to-particle transformation (Zhao et al., 2020; Almeida et al., 2013). In
62 polluted regions such as urban China, compelling evidence indicates that sulfuric acid
63 (SA)-driven nucleation enhanced by dimethylamine (DMA) can generate
64 thermodynamically stable SA-DMA clusters and lead to high particle formation rates
65 close to kinetic limit of SA clustering, which is responsible for the observed intensive
66 NPF events (Cai et al., 2021; Yao et al., 2018). Meanwhile, it has been demonstrated
67 that variations in atmospheric conditions, including condensation sinks (CS) arising
68 from background aerosols, along with temperature (T), can exert profound impacts on
69 the cluster dynamics of SA-DMA nucleation by varying the particle formation rates
70 across several orders of magnitude (Cai et al., 2021; Deng et al., 2020). Given that
71 complex interactions exist among various gaseous precursors, molecular clusters, and
72 pre-existing aerosols during nucleation, reasonable representation of the cluster
73 dynamics of SA-DMA nucleation in three-dimensional (3-D) models is important for
74 3-D NPF modeling and subsequent assessment of its impacts on environment and
75 climate.

76 Empirical models in form of power law functions have been extensively utilized to
77 examine how particle formation rates respond to precursor concentrations (Semeniuk
78 and Dastoor, 2018). Through parameter fitting, these empirical models can effectively
79 reproduce the particle formation rates observed in both laboratory experiments and field
80 measurements (Kulmala et al., 2006; Riccobono et al., 2014; Semeniuk and Dastoor,
81 2018). Subsequently, they can be integrated into 3-D models for regional or global NPF
82 simulations. Bergman et al. (2015) and Dunne et al. (2016) have simulated SA-DMA
83 nucleation utilizing global models, which incorporate empirical equations derived from
84 experimental data obtained from CLOUD chamber or flow tube experiments. These
85 parameterization schemes successfully characterize the response of particle formation
86 rates to precursor concentrations, however, they fail to account for dependencies on T
87 and CS due to the ignorance of explicit cluster dynamics. As a result, they are identified
88 to be inadequate for accurately reproducing NPF events in winter Beijing (Li et al.,
89 2023c).

90 We recently developed an analytical equation for SA-DMA nucleation
91 parameterization based on detailed cluster dynamics simulations (abbreviated as
92 `Dynamic_Sim`) (Li et al., 2023c). Previous theoretical insights into the SA-DMA
93 system (Olenius et al., 2013, 2017; Ortega et al., 2012; Myllys et al., 2019) indicate that
94 $(\text{SA})_k(\text{DMA})_k$ ($k = 1-4$) and $(\text{SA})_2(\text{DMA})_1$ clusters are considered the key clusters along
95 the cluster formation pathways in SA-DMA nucleation. Under the polluted conditions
96 ($\text{CS} > \sim 1.0 \times 10^{-2} \text{ s}^{-1}$), the evaporation rates of clusters $(\text{SA})_k(\text{DMA})_k$ ($k = 2-4$) and
97 $(\text{SA})_2(\text{DMA})_1$ clusters are negligible compared to their coagulation sink. Accordingly,
98 several simplifications have been made in `Dynamic_Sim`, including 1) only

99 (SA)_k(DMA)_k ($k = 1-4$) and (SA)₂(DMA)₁ clusters are considered; 2) clusters larger
100 than (SA)₁(DMA)₁ are regarded stable with no evaporation; and 3) (SA)₄(DMA)₄
101 cluster is the only terminal cluster in calculating particle formation rates. Subsequent
102 applications in 3-D modeling have demonstrated significantly improved performance
103 of Dynamic_Sim compared to previous data-fitting parameterizations in simulating the
104 particle formation rates, the evolution of particle number size distributions (PNSDs),
105 and NPF events in winter Beijing. However, the efficacy of Dynamic_Sim in NPF
106 simulation has yet to be assessed under varying atmospheric conditions, such as the
107 summer season characterized by relatively higher T and lower CS compared to winter.
108 Moreover, the impacts of simplifications made in the derivation of Dynamic_Sim on 3-
109 D NPF simulation under different atmospheric conditions remain unclear.

110 In addition to the form of explicit formulations, integration of nucleation dynamics
111 in 3-D models can also be realized using precomputed look-up tables generated by box
112 models. Atmospheric Cluster Dynamics Code (ACDC) is a representative box model
113 for simulating cluster dynamics and particle formation rates (Mcgrath et al., 2012;
114 Olenius et al, 2013). In addition to representing T - and CS- dependencies for particle
115 formation rate as Dynamic_Sim, ACDC considers the source/sink terms of all given
116 molecules/clusters within a nucleation system without simplifications of the clustering
117 processes. By integrating quantum chemical calculations with ACDC, Almeida et al.
118 (2013) discovered that the simulated SA-DMA nucleation provides valuable insights
119 for interpreting the measurements from the CLOUD chamber experiments. Similarly,
120 Lu et al. (2020) demonstrated that ACDC coupled with quantum chemistry calculations
121 can effectively reproduce the particle formation rates observed in urban Shanghai. In
122 addition to its extensive utilization in box modeling (Almeida et al., 2013; Lu et al.,
123 2020; Yang et al., 2021), several studies have simulated nucleation pathways in
124 chemical transport models using precomputed look-up tables generated by ACDC. For
125 example, Baranizadeh et al. (2016) and Croft et al. (2016) used ACDC-derived look-up
126 tables as nucleation parameterizations to probe the impacts of SA–NH₃–H₂O nucleation
127 on aerosol number concentration, cloud properties, and radiation balance. Olin et al.
128 (2022) and Julin et al. (2018) evaluated the impact of new particle formation on aerosol
129 number concentrations in Europe under historical and emission reduction scenarios,
130 respectively, using ACDC-derived parameterizations involving both SA–NH₃–H₂O and
131 SA-DMA nucleation. It should be noted that ACDC program in modeling the nucleation
132 process is highly reliant on specific thermodynamic data for the molecular clusters of
133 interest, which are primarily obtained through quantum chemical calculations (Elm et
134 al., 2020). A very recent study by Svenhag et al. (2024) compared the impact of two
135 typical quantum calculation methods on 3-D modeling of SA-NH₃ nucleation using
136 ACDC-derived parameterizations. However, it is still unclear how different quantum
137 chemical methods affect the 3-D modeling of SA-DMA nucleation.

138 This study aims to compare different cluster dynamic-based parameterizations for
139 SA-DMA nucleation and identify the robust one applicable for 3-D models. We
140 introduced parameterizations developed using the ACDC program, incorporating

141 various quantum chemical calculations. Different cluster dynamic-based
142 parameterizations, including ACDC-derived ones as well as Dynamic_Sim, are
143 comprehensively compared and evaluated through a combination of box-model
144 simulations, 3-D modeling, and in-situ observational data. Our findings reveal that by
145 incorporating the latest theoretical understanding and complete representation of cluster
146 dynamics, ACDC-derived parameterization demonstrates reliable performance in 3-D
147 NPF simulation for both winter and summer conditions in Beijing and exhibits potential
148 applicability in diverse atmospheric conditions. The study sheds light on the impacts of
149 employing various simplifications in cluster dynamics and different theoretical
150 approaches in deriving parameterizations on NPF simulation. In addition to
151 contributing to the precise simulation of SA-DMA nucleation and the quantification of
152 its environmental and climatic effects, this study provides valuable references for
153 simulating other nucleation mechanisms in 3-D models.

154 2 METHODS

155 2.1 Configurations of ACDC

156 Here, $(SA)_m(DMA)_n$ clusters ($0 < n \leq m \leq 3$, m and n represent the number of SA
157 and DMA molecules in a cluster) are used to build the ACDC-derived parameterizations
158 for SA-DMA nucleation due to their reported much higher stability compared to those
159 containing more DMA molecules than SA molecules (Xie et al., 2017). The ACDC code
160 is available at <https://github.com/tolenius/ACDC>. The conformations and
161 thermodynamics of SA-DMA clusters are taken from our other study (Ning et al., 2024).
162 Briefly, the conformations of selected clusters are taken from the reported global
163 minima from Li et al. (2020), and the key thermodynamic data for ACDC, Gibbs free
164 energy change (ΔG), are recalculated at the DLPNO-CCSD(T)/aug-cc-pVTZ// ω B97X-
165 D/6-311++G(3df,3pd) level of theory. Based on benchmark studies (Elm et al., 2020),
166 this level of theory provides dependable thermodynamic insights into molecular
167 clusters during nucleation and represents the latest theoretical approach. In addition, the
168 rotational symmetry is consistently considered in quantum calculations following Besel
169 et al. (2020). Following most previous ACDC simulation studies (Xie et al., 2017; Elm
170 et al., 2020; Ning et al., 2020), $(SA)_4(DMA)_3$ and $(SA)_4(DMA)_4$ clusters are defined as
171 the boundary conditions, i.e. the clusters fluxing out the simulated system and
172 participating in subsequent growth in ACDC simulations, considering their high
173 stability. Since clusters containing SA tetramers are estimated to have an electrical
174 mobility diameter of 1.4 nm (Cai et al., 2023; Jen et al., 2014; Thomas et al., 2016), the
175 formation rates of $(SA)_4(DMA)_3$ and $(SA)_4(DMA)_4$ clusters are therefore deemed as the
176 particle formation rates at 1.4 nm ($J_{1.4}$). Size-dependent coagulation sink (CoagS)
177 is counted for each SA-DMA cluster which is consistent with Dynamic_Sim (Li et al.,
178 2023c):

$$179 \text{CoagS}_i = \text{CS} \left(\frac{V_i}{V_1} \right)^{-1.7}$$

180 where V_i and V_1 (m^3) represent the volume of cluster i and SA molecule, respectively.
181 The power-law exponent of -1.7 is selected according to typical range in the atmosphere

182 (Lehtinen et al., 2007). In addition, enhancement for collision processes from Van de
183 Waals forces is also considered. We refer to the ACDC-derived parameterization in
184 coupling the DLPNO-CCSD(T)/aug-cc-pVTZ// ω B97X-D/6-311++G(3df,3pd) level of
185 theory and adequate cluster dynamics as ACDC_DB, which is established as the base-
186 case for our discussion of other cluster dynamics-based parameterizations.

187 In addition to the direct comparison of ACDC_DB to Dynamic_Sim, additional test
188 parameterizations combining ACDC_DB and three simplifications within
189 Dynamic_Sim are established and compared with ACDC_DB to further probe the
190 impacts of these simplifications on NPF simulations. According to our previous study,
191 altering the simplifications within Dynamic_Sim to explicit treatment would
192 substantially escalate the computational demand by several orders of magnitude (Li et
193 al. 2023c). Therefore, we utilize the ACDC-derived look-up tables to evaluate the
194 impacts of the simplified treatments. The configurations of all parameterizations are
195 detailed in Table 1. It should be noted that when all simplifications are applied on
196 ACDC_DB, Dynamic_Sim still predicts higher $J_{1.4}$ compared to ACDC_DB (Figure
197 S1A). This is because the ΔG value of the initial (SA)₁(DMA)₁ cluster at 298.15 K used
198 in Dynamic_Sim, which is taken from Myllys et al. (Myllys et al., 2019), is slightly
199 lower than that used in ACDC_DB (-13.5 kcal mol⁻¹ for Dynamic_Sim and -12.9 kcal
200 mol⁻¹ for ACDC_DB) (Ning et al., 2024), even though both parameterizations employ
201 the quantum chemical calculation method of DLPNO-CCSD(T). Possible reasons for
202 the discrepancy include the utilization of a larger basis set (3-zeta 6-311++G(3df,3pd))
203 and higher convergence criteria (Tight PNO + Tight SCF) in this study compared to
204 that in Myllys et al.. Aligning the ΔG for (SA)₁(DMA)₁ cluster in Dynamic_Sim with
205 that of ACDC leads to a high consistency in the predicted $J_{1.4}$ between the two
206 approaches (Figure S1B). The uncertainty of ΔG used in Dynamic_Sim is discussed in
207 our previous study (Li et al., 2023c) and here we mainly focus on the impacts of
208 simplifications in Dynamic_Sim.

209 While the DLPNO-CCSD(T)/aug-cc-pVTZ// ω B97X-D/6-311++G(3df,3pd) level
210 of theory yields reasonable cluster thermodynamics, quantum chemistry calculations
211 employing the RI-CC2 method predicting lower ΔG for cluster formation (stronger
212 binding between molecules within clusters), has been widely used in conjunction with
213 ACDC to interpret experimental and observed particle formation rates in previous
214 studies (Almeida et al., 2013; Kürten et al., 2018; Ning et al., 2020). The prevalent
215 combination used with the RI-CC2 method is RI-CC2/aug-cc-pV(T+d)Z//M06-2X/6-
216 311++G(3df,3pd) level of theory (Lu et al., 2020; Liu et al., 2021; Ning et al., 2022;
217 Ning and Zhang, 2022; Liu et al., 2019). Based on Elm's work, compared to DLPNO-
218 CCSD(T)/aug-cc-pVTZ// ω B97X-D/6-311++G(3df,3pd), the differences in predicted
219 cluster binding energies primarily stem from discrepancies between DLPNO-CCSD(T)
220 and RI-CC2 in single-point energy calculations, while the ω B97X-D and M06-2X
221 functionals exhibit similar performance (Elm et al., 2013; Elm et al., 2020). Also, in
222 previous studies the RI-CC2 method combined with ACDC was consistently
223 accompanied by application of a sticking factor (SF) of 0.5 in treating collision

224 processes (Almeida et al., 2013; Lu et al., 2020). However, it is noteworthy that,
 225 according to Stolzenburg et al.’s work (Stolzenburg et al., 2020), the SF of the neutral
 226 SA-DMA cluster system should be unity. Here, we refer to the traditional theoretical
 227 approach as employing the RI-CC2/aug-cc-pV(T+d)Z//M06-2X/6-311++G(3df,3pd)
 228 level of theory and incorporating the SF of 0.5 in collision processes. An ACDC-derived
 229 parameterization coupling the traditional theoretical approach is established to assess
 230 the effectiveness of the traditional method in NPF simulation (ACDC_RM_SF0.5).
 231 Except for the varied thermodynamic inputs and SF, the remaining configurations of
 232 ACDC_RM_SF0.5 are identical to ACDC_DB. Additionally, we establish a test
 233 parameterization coupling RI-CC2/aug-cc-pV(T+d)Z//M06-2X/6-311++G(3df,3pd)
 234 level of theory with an SF of unity (ACDC_RM) to evaluate the impact solely arising
 235 from the quantum chemical calculation method. Note that SF of unity is applied to all
 236 parameterizations in this study except for the ACDC_RM_SF0.5.

237 To quantify the differences in simulating $J_{1,4}$ among different cluster dynamics-
 238 based parameterizations compared to our base-case ACDC_DB, we introduce a
 239 parameter R :

$$240 \quad R_X = \frac{\sum_i^n (X_i / \text{ACDC_DB}_i)}{n}$$

241 where ACDC_DB_i and X_i denote the simulated $J_{1,4}$ by the base-case ACDC_DB and
 242 another specific parameterization X , respectively, given the input scenarios of i (a set
 243 of input values for T , CS, concentration of SA ($[\text{SA}]$) and DMA ($[\text{DMA}]$)), and n
 244 signifies the total number of input scenarios.

245

246 **Table 1.** Summary of various cluster dynamics-based parameterizations of SA-DMA
 247 nucleation in this study (main parameterizations are in bold, while test ones in regular)

Case	Description
Dynamic_Sim	Reported parameterization from Li et al. 2023 combining the simplifications in boundary conditions, cluster evaporations, and cluster number
ACDC_DB	ACDC-derived parameterization coupling DLPNO-CCSD(T)/aug-cc-pVTZ// ω B97X-D/6-311++G(3df,3pd) level of theory, namely the latest theoretical approach
ACDC_DB_BC	ACDC-derived parameterization coupling DLPNO-CCSD(T)/aug-cc-pVTZ// ω B97X-D/6-311++G(3df,3pd) level of theory and simplification in boundary conditions (only $(\text{SA})_4(\text{DMA})_4$ cluster is set as boundary condition)
ACDC_DB_CE	ACDC-derived parameterization coupling DLPNO-CCSD(T)/aug-cc-pVTZ// ω B97X-D/6-311++G(3df,3pd) level of theory and simplification in cluster evaporations (the evaporation rates of $(\text{SA})_k(\text{DMA})_k$ ($k = 2-3$) and $(\text{SA})_2(\text{DMA})_1$ clusters are kept zero)

ACDC_DB_CN	ACDC-derived parameterization coupling DLPNO-CCSD(T)/aug-cc-pVTZ// ω B97X-D/6-311++G(3df,3pd) level of theory and simplification in cluster number (only (SA) _k (DMA) _k ($k = 1-3$) and (SA) ₂ (DMA) ₁ clusters are involved)
ACDC_RM_SF0.5	ACDC-derived parameterization coupling RI-CC2/aug-cc-pV(T+d)Z//M06-2X/6-311++G(3df,3pd) level of theory and a SF of 0.5 is applied in collision process, namely the traditional theoretical approach
ACDC_RM	ACDC-derived parameterization coupling RI-CC2/aug-cc-pV(T+d)Z//M06-2X/6-311++G(3df,3pd) level of theory and a SF of 1 is applied

248

249 **2.2 Incorporating the ACDC-derived Parameterizations into WRF-Chem/R2D-** 250 **VBS Model**

251 Various parameterizations are subsequently implemented in the Weather Research
252 and Forecasting-Chemistry model (WRF-Chem) integrating an experimentally
253 constrained Radical Two-Dimensional Volatility Basis Set (2D-VBS) (denoted as
254 WRF-Chem/R2D-VBS) (Zhao et al., 2020). Incorporating the box-model ACDC into a
255 3-D model using the explicit mathematical formula, as Dynamic_Sim, proves to be
256 challenging. Here, we created a four-dimensional look-up table that delineates the
257 response of $J_{1,4}$ to four input variables (T , CS, [SA], and [DMA]) for each ACDC-
258 derived parameterization (Yu, 2010). The table is derived based on multiple ACDC runs
259 by varying input variables. The ranges for the input variables correspond to typical
260 conditions of the atmosphere. Except for T , the ranges of variation for all other variables
261 exceed at least one order of magnitude. Therefore, temperature is assumed to follow
262 arithmetic uniform distribution, while the other variables are assumed to follow
263 geometric uniform distribution. Details for the input variables are given in Table S1. In
264 WRF-Chem/R2D-VBS simulations, $J_{1,4}$ are online calculated by interpolating values
265 from a look-up table based on real-time input parameters. In our previous study, we
266 have developed an emission inventory for China and its surrounding regions (Li et al.,
267 2023c). Here [DMA] is calculated in WRF-Chem/R2D-VBS based on a comprehensive
268 source-sink representation of DMA. More details of including DMA in WRF-
269 Chem/R2D-VBS can be found in our previous study (Li et al., 2023c). In addition, a
270 time-integrated-average [DMA] as well as [SA] of each time step were used to drive
271 SA-DMA nucleation, since SA-DMA nucleation is accompanied with condensation of
272 gaseous SA and DMA on pre-existing aerosols simultaneously in the atmosphere.

273 Besides SA-DMA nucleation, seven other nucleation mechanisms have already
274 been incorporated in WRF-Chem/R2D-VBS (Zhao et al., 2020), including neutral/ion-
275 induced SA-H₂O nucleation, neutral/ion-induced SA-NH₃-H₂O nucleation, neutral/ion-
276 induced pure organics nucleation, and SA-organics nucleation. The organics involved
277 in nucleation are ultralow- and extremely low-volatility organic compounds (ULVOC

278 and ELVOC) with $O:C > 0.4$. The formation chemistry of ULVOC and ELVOC from
279 monoterpenes, including autoxidation and dimerization, is traced by the R2D-VBS
280 framework (Zhao et al., 2020). Note that the impact of the other seven mechanisms on
281 particle formation rates and particle number concentration is low compared to SA-DMA
282 as revealed by our previous study (Li et al., 2023c). In WRF-Chem/R2D-VBS, the
283 evolution of PNSDs from 1 nm to 10 μm is treated by MOSAIC (Model for Simulating
284 Aerosol Interactions and Chemistry) module. The newly formed 1.4 nm particles from
285 SA-DMA nucleation are injected into the smallest size bin (1 - 1.5 nm) of the MOSAIC.

286 **2.3 Configurations of WRF-Chem/R2D-VBS Model**

287 The WRF-Chem/R2D-VBS model, incorporating various cluster dynamics-based
288 SA-DMA nucleation parameterizations, was employed in a simulation over a domain
289 with a spatial resolution of 27 km. This domain covers eastern Asia, with Beijing
290 situated close to the center of the simulation area. Details of model configurations can
291 be found in our previous study (Li et al., 2023c). Briefly, we use the ABaCAS-EI 2017
292 and IIASA 2015 emission inventories for mainland China and other areas in the domain,
293 respectively, to represent the anthropogenic emissions (Zheng et al., 2019; Li et al.,
294 2017; Li et al., 2023b); we use Model of Emissions of Gases and Aerosols from Nature
295 (MEGAN) v2.04 to calculate the biogenic emissions (Guenther et al., 2006). To
296 accurately represent the variation and distribution of chemical species concentrations
297 during the simulation period, the chemical initial conditions, which represent the
298 concentration field of chemical species at the initial simulation time, and the boundary
299 conditions, which represent the flux or concentration around the simulation domain
300 during the simulation period (Brasseur et al., 2017), are used in our WRF-Chem/R2D-
301 VBS simulations. The simulation results from the National Center for Atmospheric
302 Research's Community Atmosphere Model with Chemistry
303 (<https://www.acom.ucar.edu/cam-chem/cam-chem.shtml>) is used for the chemical
304 initial and boundary conditions in WRF-Chem/R2D-VBS simulations. In addition, we
305 use a 5-day spin-up to minimize the impact of chemical initial conditions on simulation
306 results.

307 The simulation period consists of two parts: the winter period, which spans from
308 January 14 to January 31, 2019, and the summer period, which is from August 18 to
309 August 31, 2019. Previous observational studies have shown that the particle formation
310 rates reach their highest and lowest levels during winter and summer in China,
311 respectively (Deng et al., 2020; Chu et al., 2019). Therefore, periods from these two
312 seasons are selected as representative simulation periods in this study and the specific
313 time periods corresponded to those with relatively complete and continuous PNSDs and
314 $J_{1.4}$ observations. Since observational data for DMA concentration is only available for
315 the period from January 1, 2019 to January 23, 2019, similar to our other study (Ning
316 et al., 2024), we performed additional simulation for this period to compare
317 observational and simulated DMA concentrations. For each season, all the SA-DMA
318 parameterizations listed in Table 1 were employed for simulation. Among them,
319 ACDC_DB, Dynamic_Sim, and ACDC_RM_SF0.5 serve as three main

320 parameterizations, while ACDC_DB_CE, ACDC_DB_BC, ACDC_DB_CN, and
321 ACDC_RM are set as test cases to investigate the impact of individual simplification
322 or theoretical approach on NPF simulations. In all comparisons, ACDC_DB is set as a
323 reference.

324 **2.4 Ambient Measurements**

325 In the 3-D simulations, we utilize measured concentrations of nucleation precursors
326 and PNSDs as a criterion to discuss the model performance with various
327 parameterizations. The duration of the observational data matches that of the
328 simulations mentioned above. Detailed descriptions of the observation site and
329 instruments can be found in our previous research (Deng et al., 2020; Zhu et al., 2022).
330 Briefly, the observation site is located on the West Campus of the Beijing University of
331 Chemical Technology. CI-TOF-MS (chemical ionization time-of-flight mass
332 spectrometer; Aerodyne Research Inc.) were used to measure the concentrations of SA.
333 Amine concentrations were measured with a modified TOF-MS using H_3O^+ or its
334 clusters as the reagent ions (Zhu et al., 2022). PNSDs from 1 nm to 10 μm were
335 measured using a PSD (particle size distribution) system and a DEG-SMPS (diethyl
336 glycol scanning mobility particle spectrometer). $J_{1.4}$ derived from observation is
337 calculated employing an improved aerosol population balance formula (Cai and Jiang,
338 2017).

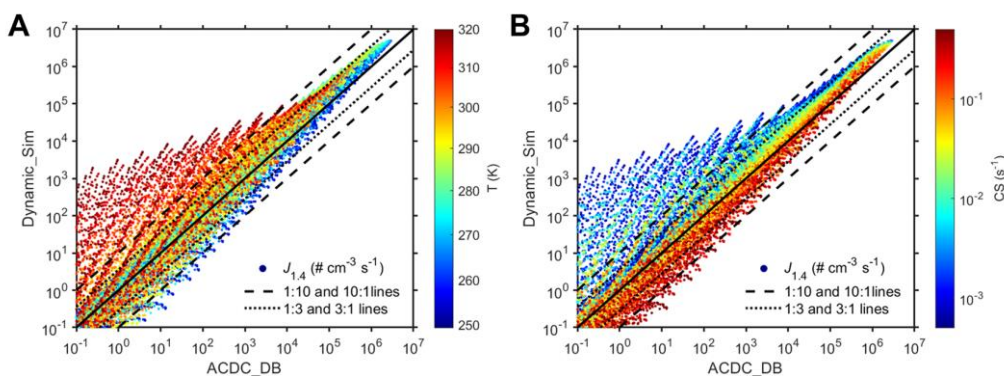
339 3 RESULTS AND DISCUSSIONS

340 3.1 Comparison of Different Parameterizations Based on Box-Model Simulations

341 3.1.1 Comparison between ACDC_DB and Dynamic_Sim

342 Figure 1 illustrates the comparison between the reported cluster dynamics-based
343 parameterization with simplifications, Dynamic_Sim, and the base-case
344 parameterization ACDC_DB. The comparison is based on a comprehensive dataset that
345 includes over 40,000 box-model simulations for each parameterization, by varying
346 parameters such as [SA] ($1 \times 10^5 - 1 \times 10^8$ molec. cm^{-3}), [DMA] ($5 \times 10^6 - 5 \times 10^8$
347 molec. cm^{-3}), CS ($5 \times 10^{-4} - 5 \times 10^{-1}$ s^{-1}), and T (250 – 320 K). In most scenarios, $J_{1,4}$
348 predicted by ACDC_DB and Dynamic_Sim demonstrates deviations within one order
349 of magnitude, with the majority falling within a factor of 3. However, Dynamic_Sim
350 predicts notably higher $J_{1,4}$ than ACDC_DB in scenarios where T exceeds ~ 300 K and
351 CS is below $\sim 3 \times 10^{-3}$ s^{-1} , characteristic of a clean atmosphere during summer. The
352 discrepancy in these scenarios elevates the overall $R_{\text{Dynamic_Sim}}$ up to 17.0. Furthermore,
353 no clear correlation is observed between the differences of the two parameterizations
354 and other input parameters such as [DMA] and [SA] (Figure S2). The differences
355 between parameterizations are attributed to the combined effects of the three
356 simplifications and the lower ΔG of $(\text{SA})_1(\text{DMA})_1$ cluster in Dynamic_Sim. However,
357 the latter should not be the primary cause for the significant differences of $J_{1,4}$ prediction
358 under high T and low CS conditions, as it typically results in an overestimation within
359 an order of magnitude ($R=3.3$) (Figure S1).

360



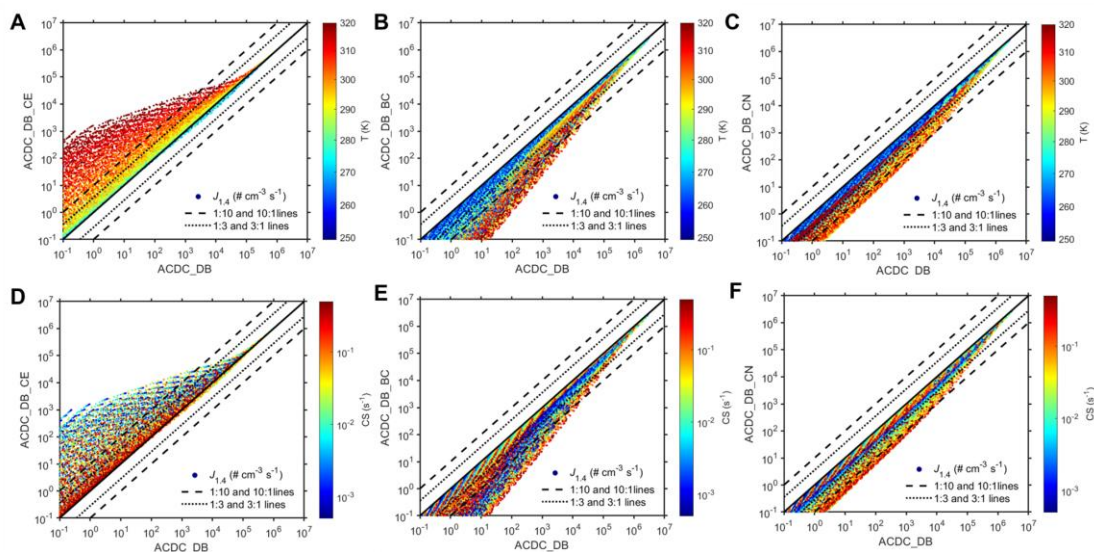
361

362 **Figure 1.** Comparison of $J_{1,4}$ predictions between ACDC_DB and Dynamic_Sim
363 correlated with T variation (A) and CS variation (B). Solid dots represent simulated $J_{1,4}$
364 values, solid lines indicate a 1:1 line, dotted lines correspond to 1:3 and 3:1 lines,
365 and dashed lines represent 1:10 and 10:1 lines.

366

367 The impacts of the three simplifications made in Dynamic_Sim are shown in Figure
368 2. Specifically, the simplification in cluster evaporations tends to elevate the predicted
369 $J_{1,4}$, whereas the simplifications in boundary conditions and cluster number tend to
370 lower them. When applying the simplification in cluster evaporations (clusters larger
371 than $(\text{SA})_1(\text{DMA})_1$ are regarded stable with no evaporation) to ACDC_DB, the
372 predicted $J_{1,4}$ by ACDC_DB_CE only slightly exceed than that of ACDC_DB within a

373 factor of 3 under conditions where $T < \sim 290$ K and $CS > \sim 0.1$ s⁻¹. However, the
374 overestimation of $J_{1,4}$ prediction by ACDC_DB_CE becomes much greater with
375 increasing T and decreasing CS . The discrepancy between ACDC_DB_CE and
376 ACDC_DB should be primarily attributed to the pivotal role of T in influencing cluster
377 evaporation rates (Ortega et al., 2012; Deng et al., 2020). At low T , the evaporation
378 rates of clusters are low enough to allow efficient nucleation, thus whether setting the
379 concerned SA-DMA clusters to evaporate based on the expected evaporation rates does
380 not lead to a significant impact on $J_{1,4}$ prediction. However, at high T , the evaporation
381 rates of clusters significantly increase, therefore the simplification in cluster
382 evaporations within ACDC_DB_CE is likely to predict higher $J_{1,4}$ than those with no
383 simplification. The impact of simplification in cluster evaporations across varying T is
384 also found in a nonbranched SA-DMA nucleation scheme from 280 K to 298 K reported
385 by Li et al. (2023a). Note also that the overestimation of ACDC_DB_CE diminishes as
386 CS increases (Figure 2D), with CS becoming the primary sink in the nucleation system
387 and the impact of cluster evaporations becoming less pronounced. This underscores the
388 connection between the specific deviation arising from simplification in cluster
389 evaporations and the respective contributions of CS and cluster evaporations to the
390 overall sink for clusters in nucleation. In addition, the relative independence of the
391 differences between ACDC_DB_CE and ACDC_DB from variations in precursor
392 concentrations ($[SA]$ and $[DMA]$) is similar to that between Dynamic_Sim and
393 ACDC_DB (Figure S3). Overall, the scenarios where ACDC_DB_CE predicts higher
394 $J_{1,4}$ than ACDC_DB only occurs under conditions of both high T and low CS (Figure
395 2A and Figure 2D). The averaged discrepancy between ACDC_DB_CE and
396 ACDC_DB $R_{ACDC_DB_CE}$ is 22.3, closely resembling $R_{Dynamic_Sim}$, indicating that the
397 simplification in cluster evaporations is a major factor contributing to the difference
398 between Dynamic_Sim and ACDC_DB.
399
400



401
402 **Figure 2.** Comparison of $J_{1,4}$ predictions between ACDC_DB and test cases including

403 ACDC_DB_CE (A and D), ACDC_DB_BC (B and E), and ACDC_DB_CN (C and F).
404 The first row in the panel (A, B and C) is correlated with T variation and the second
405 row (D, E and F) is correlated with CS variation. Solid dots represent simulated $J_{1.4}$
406 values, solid lines indicate a 1:1 line, dotted lines correspond to 1:3 and 3:1 lines, and
407 dashed lines represent 1:10 and 10:1 lines.

408

409 The underestimations of ACDC_DB_BC and ACDC_DB_CN in $J_{1.4}$ prediction
410 compared to base-case ACDC_DB are related to the growth pathways of SA-DMA
411 clusters. In the original scheme of ACDC_DB, precursor molecules have the flexibility
412 to pass through any $(SA)_m(DMA)_n$ clusters ($0 < n \leq m \leq 3$), and terminal 1.4-nm
413 particles are formed when the clusters grow to $(SA)_4(DMA)_4$ or $(SA)_4(DMA)_3$. As
414 expected, ACDC_DB_BC, which assumes $(SA)_4(DMA)_4$ cluster as the only boundary
415 condition with an omission of $(SA)_4(DMA)_3$ cluster, predicts lower $J_{1.4}$ than ACDC_DB.
416 $(SA)_4(DMA)_3$ and $(SA)_4(DMA)_4$ clusters are primarily formed from $(SA)_3(DMA)_3$
417 cluster by colliding with a SA molecule and a $(SA)_1(DMA)_1$ cluster, respectively. As
418 the concentration of $(SA)_1(DMA)_1$ cluster is more sensitive to T , we further found that
419 the discrepancy between ACDC_DB_BC and ACDC_DB becomes more pronounced
420 with increasing T (Figure 2B). Furthermore, we found no apparent correlation between
421 the variation of CS and the disparity between ACDC_DB_BC and ACDC_DB (Figure
422 2E).

423 In addition to ACDC_DB_BC, ACDC_DB_CN also underestimates $J_{1.4}$ compared
424 to ACDC_DB with a comparable value (~ 0.5) of $R_{ACDC_DB_CN}$ and $R_{ACDC_DB_BC}$. Under
425 the simplification in cluster number, the formation of 1.4-nm clusters can only occur
426 through specific pathways, including $(SA)_1(DMA)_1 \rightarrow (SA)_2(DMA)_2 \rightarrow (SA)_3(DMA)_3$
427 $\rightarrow (SA)_4(DMA)_4/(SA)_4(DMA)_3$, $(SA)_1(DMA)_1 \rightarrow (SA)_2(DMA)_1 \rightarrow (SA)_2(DMA)_2 \rightarrow$
428 $(SA)_3(DMA)_3 \rightarrow (SA)_4(DMA)_4/(SA)_4(DMA)_3$, or a combination thereof, while other
429 pathways are restricted. Due to the variability in growth pathways and their
430 contributions to $J_{1.4}$ under different atmospheric conditions, the difference between
431 ACDC_DB_CN and ACDC_DB is not strongly correlated with the variations of T and
432 CS (Figure 2C and Figure 2F). Despite that, while the differences between the two
433 tested parameterizations (ACDC_DB_BC and ACDC_DB_CN) involving cluster
434 growth pathways and the original ACDC_DB are not highly correlated with [DMA],
435 there is a more pronounced correlation with [SA], which implies a more important role
436 of SA in cluster growth (Figure S4 and Figure S5).

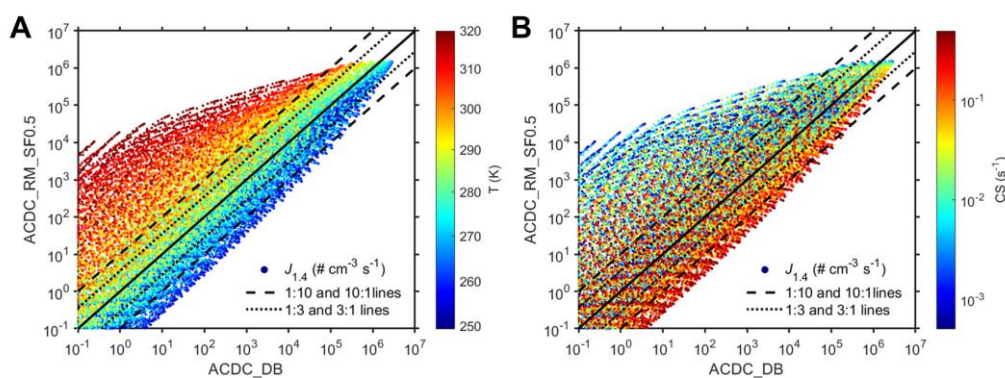
437 In our previous study, we demonstrated improvements in computing CS- dependent
438 $J_{1.4}$ of SA-DMA nucleation with the Dynamic_Sim compared to the previous power-
439 law parameterizations under polluted atmospheric conditions (Li et al., 2023c). Here,
440 we further show that, based on Dynamic_Sim, the new ACDC_DB with complete
441 cluster dynamics can more reasonably simulate $J_{1.4}$ under previously less studied
442 conditions of high T ($> \sim 300$ K) and low CS ($< \sim 3 \times 10^{-3} \text{ s}^{-1}$), where Dynamic_Sim tends
443 to produce significant overestimation of $J_{1.4}$. This overestimation is primarily driven by
444 the simplification in cluster evaporations within Dynamic_Sim. Even though a

445 comparable performance in $J_{1,4}$ prediction between ACDC_DB and Dynamic_Sim
 446 could be achieved under other ambient conditions, cautions should be made that the
 447 mutual offsetting effect between overestimation and underestimation resulting from
 448 different simplifications in Dynamic_Sim when computing $J_{1,4}$.

449 3.1.2 Comparison between ACDC_DB and ACDC_RM_SF0.5

450 In Figure 3, ACDC_DB is compared with another main ACDC-derived
 451 parameterization, ACDC_RM_SF0.5, which uses the RI-CC2/aug-cc-pV(T+d)Z//M06-
 452 2X/6-311++G(3df,3pd) level of theory and employs a SF of 0.5 in processing collision.
 453 It can be observed that at lower temperatures (~ 280 K), ACDC_RM_SF0.5 and
 454 ACDC_DB exhibit similar performance in predicting $J_{1,4}$. However, with higher T
 455 (accompanied by lower CS with a slight dependency), $J_{1,4}$ predicted by
 456 ACDC_RM_SF0.5 become higher than that predicted by ACDC_DB, reaching even
 457 several orders of magnitude at the upper limit of the T range (320 K). Furthermore, we
 458 also observed that in scenarios close to the lower limit of the T range (250 K), the $J_{1,4}$
 459 predicted by ACDC_RM_SF0.5 shift from being higher to lower compared to
 460 ACDC_DB.

461



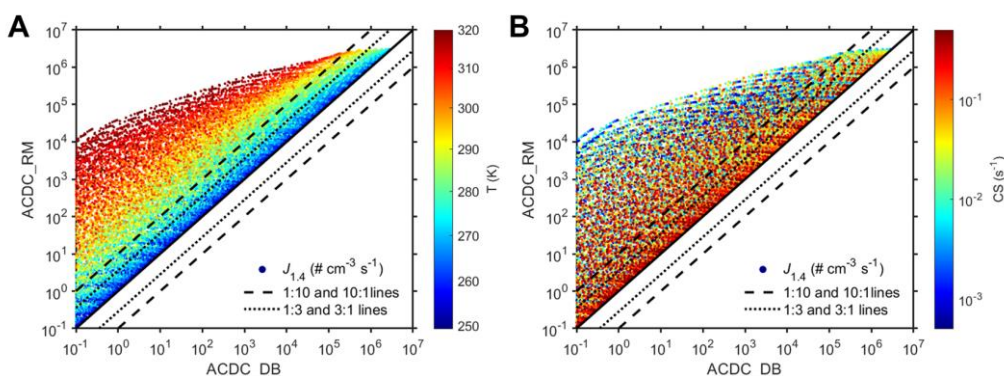
462

463 **Figure 3.** Comparison of $J_{1,4}$ predictions between ACDC_DB and ACDC_RM_SF0.5
 464 correlated with T variation (A) and CS variation (B). Solid dots represent simulated $J_{1,4}$
 465 values, solid lines indicate a 1:1 line, dotted lines correspond to 1:3 and 3:1 lines, and
 466 dashed lines represent 1:10 and 10:1 lines.

467

468 The distinction between ACDC_RM_SF0.5 and ACDC_DB arises from the
 469 combined effects of variation in quantum chemical calculation method and the
 470 application of the 0.5 SF in collision processing. As depicted in Figure 4, when the SF
 471 in ACDC_RM_SF0.5 is set to unity as in ACDC_DB, the resulting ACDC_RM
 472 parameterization predicts consistently higher $J_{1,4}$ than ACDC_DB. This implies that the
 473 modified quantum chemical calculation method, which results in lower evaporation
 474 rates for clusters within the system compared to ACDC_DB under the same condition,
 475 leads to higher $J_{1,4}$ predictions. The impact from varying quantum chemical calculation
 476 method is akin to that from simplification in cluster evaporations discussed earlier. The
 477 distinction between ACDC_RM and ACDC_DB_CE lies in the fact that the modified
 478 quantum chemical calculation method affects all clusters within the system, whereas

479 the simplification in cluster evaporations is specific to limited clusters. This contributes
 480 to a much higher R_{ACDC_RM} (614.5) compared to $R_{ACDC_DB_CE}$ (22.3). Despite that,
 481 compared to ACDC_DB, the differences for both ACDC_DB_CE, ACDC_RM, as well
 482 as ACDC_RM_SF0.5 demonstrate similar sensitivity to T (Figure 3A and Figure 4A)
 483 and CS (Figure 3B and Figure 4B) but independence on [SA] (Figure S6A and Figure
 484 S7A) and [DMA] (Figure S6B and Figure S7B). Comparing ACDC_RM_SF0.5 and
 485 ACDC_RM, it can be inferred that the application of a 0.5 SF in collision processes
 486 would result in an underestimation in $J_{1.4}$ prediction. It can be noted that in most
 487 previous studies (Almeida et al., 2013; Kürten et al., 2018; Elm et al., 2020),
 488 comparisons of ACDC simulations using the traditional method and measured particle
 489 formation rates are conducted at around 280 K. At this temperature, all three main
 490 parameterizations of ACDC_RM_SF0.5, ACDC_DB, and Dynamic_Sim tends to yield
 491 similar $J_{1.4}$ predictions and should have consistent applicability in NPF simulation.
 492



493
 494 **Figure 4.** Comparison of $J_{1.4}$ predictions between ACDC_DB and ACDC_RM
 495 correlated with T variation (A) and CS variation (B). Solid dots represent simulated $J_{1.4}$
 496 values, solid lines indicate a 1:1 line, dotted lines correspond to 1:3 and 3:1 lines,
 497 and dashed lines represent 1:10 and 10:1 lines.

498
 499 In summary, based on our base-case parameterization ACDC_DB, the extensive
 500 box-model simulations above demonstrate the characteristics of different
 501 parameterizations. Specifically, Dynamic_Sim shows general consistency with
 502 ACDC_DB in simulating $J_{1.4}$ under most atmospheric conditions with $T < \sim 300$ K or
 503 $CS > \sim 3.0 \times 10^{-3} \text{ s}^{-1}$ while overestimating $J_{1.4}$ with $T > \sim 300$ K and $CS > \sim 3.0 \times 10^{-3} \text{ s}^{-1}$
 504 compared to ACDC_DB. ACDC_RM_SF0.5 performs similarly to ACDC_DB under
 505 conditions of ~ 280 K but give different $J_{1.4}$ predictions at other temperatures. We
 506 further use reported measurements from well-controlled CLOUD chamber experiments
 507 to examine the characteristics and applicability of these parameterizations (Xiao et al.,
 508 2021). As shown in Figure S8, simulated $J_{1.4}$ using three main parameterizations,
 509 ACDC_DB, ACDC_RM_SF0.5, and Dynamic_Sim, correspond well to measured $J_{1.7}$
 510 at low temperature ($T = 278$ K), proving the applicability of all three parameterizations
 511 at this temperature. In the experiments with elevated temperature ($T = 293$ K),
 512 ACDC_DB and Dynamic_Sim continues to exhibit similar performance, with slight

513 overestimation by approximately 2 factors. This may be because the much lower cluster
514 concentrations at high temperatures compared to those at low temperatures lead to
515 slower cluster growth and thus an enlarged gap between $J_{1.4}$ and $J_{1.7}$ (Figure S9). In
516 contrast, ACDC_RM_SF0.5 only shows a slight T -dependence, which is deviated from
517 the measurements. The comparison between controlled experiments and box-model
518 simulations hence confirms our conclusions above, and provides a solid basis for further
519 discussions on 3-D simulations using these parameterizations with constraint from field
520 observations.

521 **3.2 Comparison of Different Parameterizations Based on 3-D Model Simulations**

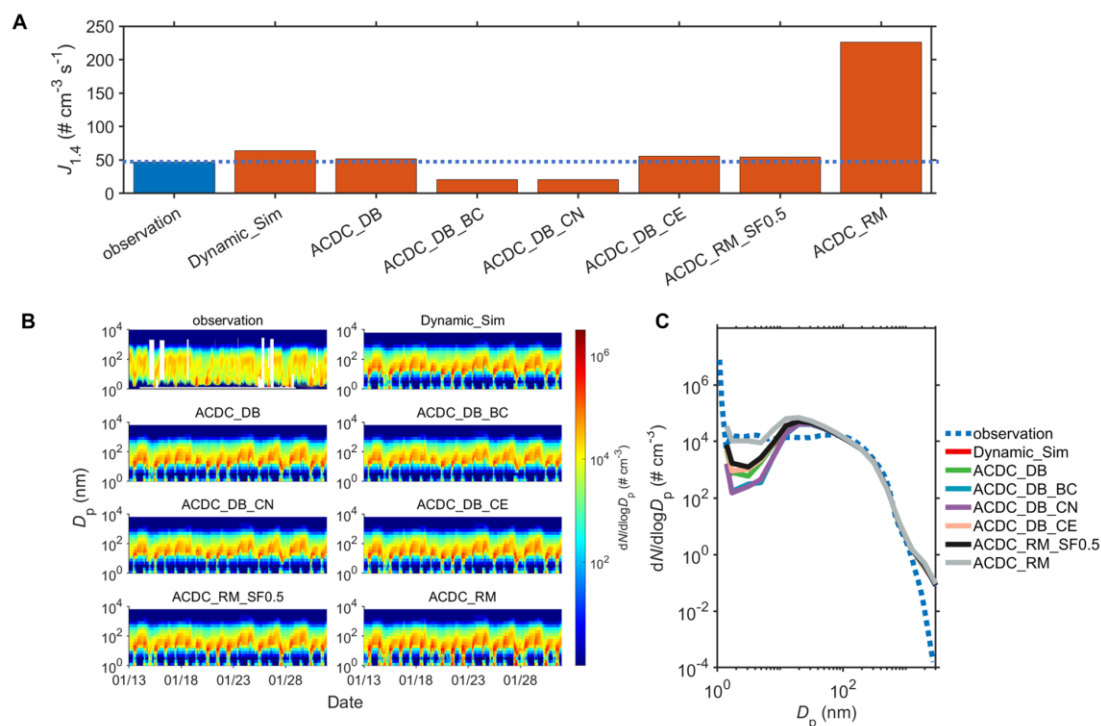
522 Various cluster dynamics-based parameterizations for SA-DMA nucleation were
523 subsequently integrated into the WRF-Chem/R2D-VBS model. 3-D simulations using
524 these parameterizations have been conducted for both wintertime and summertime
525 conditions in Beijing. Given that the concentrations of precursors are crucial input
526 variables for each parameterization, the simulated and observed concentrations of
527 [DMA] and [SA] are compared. Figure S10, Figure S11 and Table S2 illustrates good
528 consistencies in temporal variations and the mean values between simulations and
529 observations in Beijing. This validates the reliability of our representation of sources
530 and sinks for nucleating precursors and serves as a foundation for our discussions on
531 the performances of various parameterizations. In the following sections, we discuss
532 the results of 3-D NPF simulations in Beijing during winter and summer by employing
533 different parameterizations. The evaluation of various parameterizations focuses on
534 their ability to reproduce in situ NPF measurements across different seasons.

535 **3.2.1 Wintertime Simulations**

536 Figure 5A and Figure S12A primarily compare the simulated $J_{1.4}$ values from
537 different parameterizations with those derived from wintertime observations in Beijing,
538 as $J_{1.4}$ being a key parameter describing NPF events. The performance of Dynamic_Sim
539 in simulating $J_{1.4}$ during wintertime Beijing has been discussed in our previous study
540 (Li et al., 2023c). The averaged $J_{1.4}$ simulated by three main parameterizations
541 (Dynamic_Sim: $64.0 \text{ cm}^{-3} \text{ s}^{-1}$; ACDC_DB: $51.6 \text{ cm}^{-3} \text{ s}^{-1}$; ACDC_RM_SF0.5: 54.5 cm^{-3}
542 s^{-1}) approximate the observation ($46.7 \text{ cm}^{-3} \text{ s}^{-1}$). For test cases, however, only
543 ACDC_DB_CE ($55.7 \text{ cm}^{-3} \text{ s}^{-1}$) demonstrates a reasonable representation of $J_{1.4}$. $J_{1.4}$
544 simulated from ACDC_DB_BC ($20.5 \text{ cm}^{-3} \text{ s}^{-1}$) and ACDC_DB_CN ($20.8 \text{ cm}^{-3} \text{ s}^{-1}$) are
545 approximately two times lower than the observed values, while ACDC_RM (226.2 cm^{-3}
546 s^{-1}) is approximately five times higher than the observations.

547 The performances of different parameterizations on depicting $J_{1.4}$ subsequently
548 influences their representations of PNSDs evolution and NPF events, which are shown
549 in Figure 5B. Generally, most parameterizations efficiently reproduce the observed time
550 evolution of PNSDs and captures NPF events, such as those on 01/20, 01/21, 01/30,
551 and 01/31, which are characterized by the burst of aerosol number concentrations in
552 nanometer-sized range. Simulations using ACDC_DB_BC and ACDC_DB_CN result
553 in lower particle concentrations in the low size range (1-10 nm) during the NPF period
554 compared to three main parameterizations and the observations, while simulations with

555 ACDC_RM show higher concentrations. This is consistent with the comparison of $J_{1.4}$
 556 among different parameterizations and further evident by the comparison of averaged
 557 PNSDs in Figure 5C. Notably, when compared to observations, all parameterizations
 558 consistently underestimate the averaged PNSDs within the 2-10 nm range but
 559 overestimate them in the 10-50 nm range. This discrepancy may stem from simplified
 560 assumptions in particle growth simulation, as discussed in our previous study (Li et al.,
 561 2023c).
 562
 563



564
 565 **Figure 5.** Comparison of simulated particle formation rates and particle number size
 566 distributions (PNSDs) with observations during January 13, 2019, to January 31, 2019,
 567 in Beijing. A represents the averaged particle formation rates during the period, the blue
 568 bars and orange bars represent observations and simulations, respectively, while the
 569 blue dashed line represents the observed values. Daily maximum values of $J_{1.4}$ are used
 570 following Deng et al. (2020); B for the time series of PNSDs; and C for the averaged
 571 PNSDs.

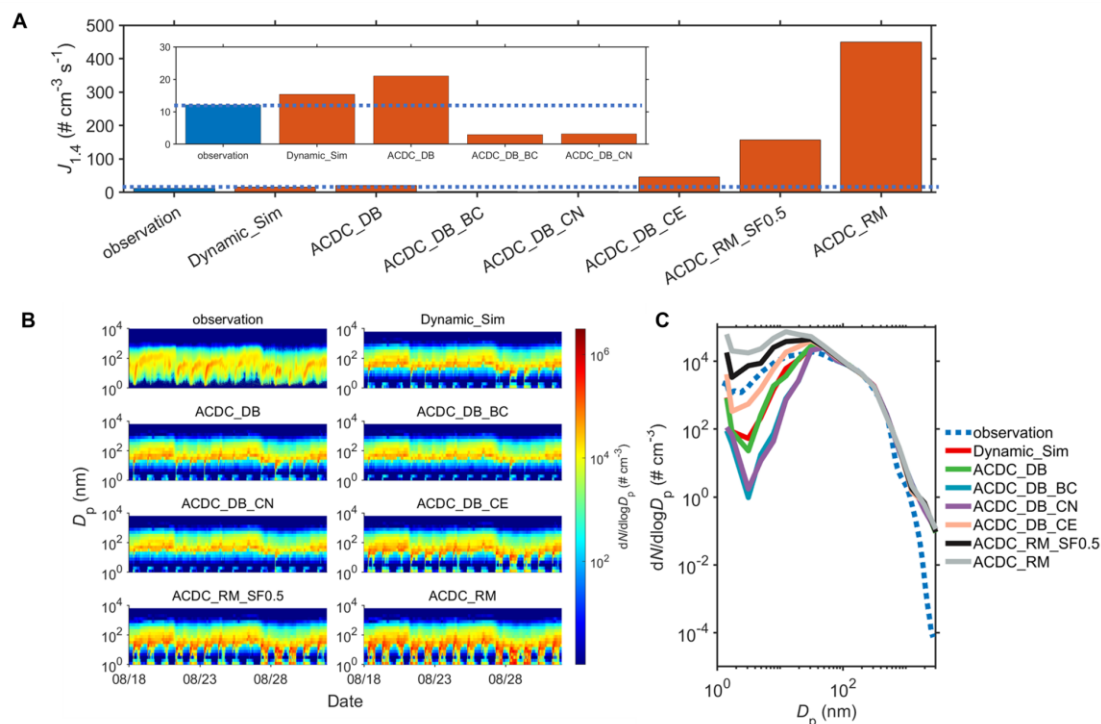
572
 573 The results show the applicability of all three main parameterizations in NPF
 574 modeling during wintertime periods. Importantly, the reliability of the new ACDC-
 575 derived parameterization based on the latest theoretical approach (ACDC_DB) without
 576 simplifications in 3-D NPF simulation, is affirmed. The differences among various
 577 parameterizations can be explained by the comprehensive box-model simulations
 578 above at corresponding conditions. Compared to ACDC_DB, the $J_{1.4}$ and PNSDs
 579 simulated by other two main parameterizations (Dynamic_Sim and ACDC_RM_SF0.5)
 580 agree similarly with observations, but for different reasons. In the case of Dynamic_Sim,

581 the simplification in cluster evaporations has minimal impact on NPF simulation since
582 CS is the dominant sink for clusters under the wintertime conditions (averaged T and
583 CS is 274.7 K and $3.3 \times 10^{-2} \text{ s}^{-1}$, respectively). However, the simplifications in boundary
584 conditions and cluster number lead to the underestimation of the $J_{1.4}$, consequently
585 lowering the simulated particle number concentrations in 1-100 nm size range due to
586 the ignorance of clusters contributing to growth. As a result, the agreement of
587 Dynamic_sim to observations should result from a combination of underestimation due
588 to simplifications in boundary conditions and cluster number, along with the
589 compensatory effect of the overestimation caused by lower ΔG for (SA)₁(DMA)₁
590 cluster. For another main parameterization ACDC_RM_SF0.5, since the test
591 parameterization ACDC_RM considerably overestimates $J_{1.4}$ and PNSDs compared to
592 the observations, the general agreement between ACDC_RM_SF0.5 and observations
593 should be attributed to a balance between reduced kinetic limit through the application
594 of SF and the compensatory effect of the overestimation caused by inappropriate
595 representation of cluster thermodynamics.

596 3.2.2 Summertime Simulations

597 Figure 6 provides additional insight into the performance of various
598 parameterizations in NPF simulation during summer. It can be noted that there exists a
599 significant difference in particle formation rates between winter and summer in Beijing.
600 As shown in Figure 6 and Figure S12B, ACDC_DB and Dynamic_Sim continues to
601 demonstrate consistent and effective performance in simulating $J_{1.4}$ (within a factor of
602 2), PNSDs evolution as well as NPF events. However, distinct differences emerge in
603 the NPF simulation for other parameterizations, including another main
604 parameterization ACDC_RM_SF0.5. Specifically, in contrast to the good performance
605 of ACDC_DB and Dynamic_Sim, ACDC_RM_SF0.5, along with the test case
606 ACDC_RM, exhibits a significant overestimation of $J_{1.4}$, exceeding the observations by
607 more than 15 times and over two orders of magnitude, respectively. This aligns with
608 their overestimation of NPF occurrences and particle number concentration in the size
609 range of 1-100 nm in comparison to observation, with a more pronounced
610 overestimation for ACDC_RM. Conversely, the test cases of ACDC_DB_BC and
611 ACDC_DB_CN show an underestimation of averaged $J_{1.4}$ by approximately 4-5 times.
612 They almost fail to depict NPF events, resulting in a significant underestimation of
613 number concentrations in the 1-100 nm size range. Simulations using ACDC_DB_CE
614 notably overestimates $J_{1.4}$ especially on 08/28 – 08/31 (Figure S11B), which results in
615 an overestimation of averaged $J_{1.4}$ by approximately 4 times compared to the
616 observations. However, apart from a moderate overestimation in the initial particle size,
617 we can observe a closer alignment of particle number concentrations in the 2-50 nm
618 range with observations for ACDC_DB_CE, which should result from a combination
619 of surplus newly formed particles and fast particle growth from inadequate assumptions
620 within the model. For the broader 2-100 nm size range, it can be observed that
621 ACDC_DB and Dynamic_Sim are closer to the observations compared to
622 ACDC_DB_CE and another major parameterization ACDC_RM_SF0.5 (Figure S13).

623 The latter two overestimate the average number concentrations during the simulation
 624 period by 1.6 times and 2.5 times, respectively. Given the more accurate representation
 625 of nucleation rates by ACDC_DB and Dynamic_Sim, the discrepancies in the 2-100
 626 nm size range compared to the observed PNSDs should also stem from the simplified
 627 assumptions in particle growth simulations.



628
 629 **Figure 6.** Comparison of simulated particle formation rates and particle number size
 630 distributions (PNSDs) with observations during August 18, 2019, to August 31, 2019,
 631 in Beijing. A represents the averaged particle formation rates during the period, the blue
 632 bars and orange bars represent observations and simulations, respectively, while the
 633 blue dashed line represents the observed values. Daily maximum values of $J_{1,4}$ are used
 634 following Deng et al. (2020); B for the time series of PNSDs; and C for the averaged
 635 PNSDs.

636
 637 Most previous NPF studies combining experiments/observations with simulations
 638 are conducted under conditions biased towards winter ($\sim 280\text{K}$) (Almeida et al., 2013;
 639 Lu et al., 2020). Under summer conditions with elevated T , there exists a deficiency in
 640 parameterization evaluations for simulating NPF. The 3-D simulation results during the
 641 summer period provide additional validation for the reliability of ACDC_DB. For
 642 ACDC_RM_SF0.5, evidence from both box-model simulations and 3-D simulations
 643 suggests that it can accurately reproduce real SA-DMA nucleation at temperatures
 644 around 280 K, while it has limitations in higher temperatures. Another main
 645 parameterization Dynamic_Sim consistently demonstrates good performance in NPF
 646 simulation, akin to its efficacy in winter conditions. With the increased temperature in
 647 summer (averaged T is 298.2 K), the influence of simplifications in cluster evaporations,
 648 cluster number, and boundary conditions becomes more profound, mirroring the trends

649 observed in box-model simulations above. This leads to more significant
650 overestimation for ACDC_DB_CE, and underestimation for ACDC_DB_CN and
651 ACDC_DB_BC compared to the observation as well as the base-case ACDC_DB. Note
652 that CS during the summer period (averaged CS is $2.8 \times 10^{-2} \text{ s}^{-1}$) decreases compared to
653 winter but remains significantly higher than typical values in clean regions ($\sim 3.0 \times 10^{-3}$
654 s^{-1}) (Dal Maso et al., 2008). According to the limited conditions for Dynamic_Sim
655 described above, although the overestimation of $J_{1.4}$ prediction resulting from the
656 simplification in cluster evaporations is more pronounced in summer compared to that
657 in winter, impacts from diverse overestimations and underestimations from different
658 simplifications and varied thermodynamics for (SA)₁(DMA)₁ cluster can still offset
659 each other, thereby allowing Dynamic_Sim to match observations. Based on previous
660 comparisons using box-models, significant differences in $J_{1.4}$ predictions between
661 Dynamic_Sim and ACDC_DB only exist under conditions of high $T > \sim 300 \text{ K}$ and low
662 $\text{CS} < \sim 3 \times 10^{-3} \text{ s}^{-1}$, thus similar performance of Dynamic_Sim and ACDC_DB can be
663 expected in the polluted atmosphere ($\text{CS} > \sim 1.0 \times 10^{-2} \text{ s}^{-1}$). In clean atmosphere with
664 high temperature, however, caution is advised when using Dynamic_Sim for 3-D NPF
665 simulations.

666 4. CONCLUSIONS and DISCUSSIONS

667 By integrating box modeling, 3-D simulations, also under the constraint from in
668 situ measurements, this study conducts comprehensive comparison of different cluster
669 dynamics-based parameterizations for SA-DMA nucleation. Among them, the ACDC-
670 derived parameterization grounded in the latest molecular-level understanding and
671 complete representation of cluster dynamics (ACDC_DB), is identified to effectively
672 model particle formation rates and PNSDs evolution in both winter and summer in
673 Beijing within 3-D simulations. While a previously proposed simplified cluster
674 dynamics-based parameterization (Dynamic_Sim) performs comparably in modeling
675 NPF in Beijing, analysis reveals that their similarity arises from a delicate balance
676 between overestimation and underestimation due to simplifications in cluster dynamics
677 processes and the difference in thermodynamics of initial cluster. Particularly, under
678 specific conditions of high temperature ($> \sim 300 \text{ K}$) and low CS ($< \sim 3 \times 10^{-3} \text{ s}^{-1}$),
679 Dynamic_Sim tends to make significant overestimation of particle formation rates
680 compared to the reality. Moreover, the study furnishes evidence that integrating ACDC-
681 derived parameterizations with the traditional theoretical approach RI-CC2/aug-cc-
682 pV(T+d)Z//M06-2X/6-311++G(3df,3pd) (ACDC_RM_SF0.5) effectively captures
683 particle formation rates and the evolution of PNSDs around 280 K, a temperature range
684 frequently explored in prior experiments and simulations investigating NPF (Kirkby et
685 al., 2011; Almeida et al., 2013; Kirkby et al., 2016; Xie et al., 2017; He et al., 2021; Ma
686 et al., 2019). Therefore, ACDC_RM_SF0.5 exhibits consistent applicability as other
687 two parameterizations at around $\sim 280 \text{ K}$. However, attributed to an inappropriate
688 representation of cluster thermodynamics, ACDC_RM_SF0.5 has limitations in
689 predicting particle formation rates at elevated temperatures. Overall, considering all

690 aspects, we recommend ACDC_DB as a more reliable parameterization for simulating
691 NPF across various atmospheric environments.

692 In addition to contributing to a more reasonable 3-D modeling of NPF, our research
693 further provides valuable references for the development of parameterizations for other
694 nucleation systems. Firstly, we demonstrate the efficacy of the DLPNO-CCSD(T)/aug-
695 cc-pVTZ// ω B97X-D/6-311++G(3df,3pd) level of theory in describing the
696 thermodynamic properties of SA-DMA clusters through comprehensive evidence. This
697 approach can thus be referenced when using quantum chemical calculations to obtain
698 thermodynamic data for other nucleation clusters, especially for other alkylamines such
699 as methylamine/trimethylamine-sulfuric acid clusters. Although DLPNO method still
700 has uncertainties in accurately describing cluster thermodynamics (Besel et al., 2020),
701 it is well recognized as the best available method currently (Elm et al., 2020). Besides,
702 in some qualitative studies, e.g., comparing the enhancing potential or synergistic
703 effects of different precursors in SA-driven nucleation, methods other than DLPNO-
704 CCSD(T)/aug-cc-pVTZ// ω B97X-D/6-311++G(3df,3pd), such as RI-CC2/aug-cc-
705 pV(T+d)Z//M06-2X/6-311++G(3df,3pd), are equally valid (Liu et al., 2019).

706 Comprehensive modeling evidences are provided in this study that certain
707 simplifications or assumptions in cluster dynamics, such as reducing the number of
708 expected clusters, modifying boundary conditions, and assuming certain clusters to be
709 non-evaporative, can significantly impact the prediction of particle formation rates and
710 hence alter the 3-D NPF simulation under certain conditions. While applying certain
711 simplifications concurrently under specific ambient conditions can offset different
712 influences against each other, leading to a satisfactory model-observation comparison,
713 there is a risk that certain simplifications may drive the model's outcomes away from
714 reality when environmental conditions change. Therefore, caution should be exercised
715 when applying these simplifications in derivation of nucleation parameterizations and
716 subsequent application in 3-D models. In addition to the simplifications within the
717 cluster dynamics regime, it should be noted that current standard treatments in 3-D
718 models that ignore detailed gas-cluster-aerosol interactions may also lead to biases
719 under certain atmospheric conditions (Olenius and Roldin, 2022). This applies not only
720 to parameterizations involving explicit mathematical expressions but also to those using
721 ACDC-derived look-up tables. Additional evaluations for the SA-DMA system indicate
722 that the impacts of these treatments may be highest under a combination of low
723 temperature ($< \sim 270$ K), low CS ($< \sim 0.003$ s⁻¹), and low precursor concentrations,
724 which leads to elevated time to reach steady state and a higher proportion of precursor
725 consumption from cluster formation, as also indicated by Olenius and Roldin's study
726 (Olenius and Roldin, 2022). Despite these impacts being generally limited under most
727 atmospheric conditions in our modeling scenarios (see supporting information), further
728 research, especially using computationally lightweight models, should aim to
729 circumvent the potential bias by linking the cluster and aerosol dynamics (Olenius and
730 Roldin, 2022).

731 It is recognized that the development of cluster dynamics-based nucleation
732 parameterizations in the form of explicit mathematical expressions is subject to
733 limitations, especially for systems involving multiple precursor species (Semeniuk and
734 Dastoor, 2018). Given that the original ACDC has been extended to involve more than
735 two precursor species, the ACDC-derived parameterization framework, in the form of
736 a look-up table, is highly meaningful for establishing parameterizations for these multi-
737 component nucleation systems. Given that multiple nucleation pathways may be
738 simultaneously considered and simulated in 3-D modeling through ACDC-derived
739 look-up tables, automatized incorporation of tables are needed through useful tools such
740 as J-GAIN developed recently (Yazgi and Olenius, 2023).

741 **Appendix.** Abbreviations used in the main text.
742
743 **SA:** sulfuric acid
744 **DMA:** dimethylamine
745 **ACDC:** Atmospheric Cluster Dynamic Code
746 **DB:** DLPNO-CCSD(T)/aug-cc-pVTZ// ω B97X-D/6-311++G(3df,3pd) level of theory
747 **RM:** RI-CC2/aug-cc-pV(T+d)Z//M06-2X/6-311++G(3df,3pd) level of theory
748 **CE:** simplification in cluster evaporations (only $(SA)_k(DMA)_k$ ($k = 1-4$) and
749 $(SA)_2(DMA)_1$ clusters are considered)
750 **CN:** simplification in cluster number (clusters larger than $(SA)_1(DMA)_1$ are regarded
751 stable with no evaporation)
752 **BC:** simplification in boundary conditions ($(SA)_4(DMA)_4$ cluster is set as the only
753 terminal cluster in calculating particle formation rates)
754 **SF:** sticking factor used in collision process
755 **Dynamic_Sim:** a reported cluster-dynamic based parameterization incorporating
756 simplifications of CE, CN and BC.
757 **$J_{1.4}$:** particle formation rate at 1.4 nm
758 **R:** a parameter to quantify the differences in simulating $J_{1.4}$ among different cluster
759 dynamics-based parameterizations compared to the base-case ACDC_DB

760 **Code and data availability.** The data and code used in this study are available upon
761 request from the corresponding author.

762

763 **Author contributions.** JS, BZ, and SW designed the research; AN and XZ collected
764 the quantum chemistry calculation data; JS performed the ACDC and WRF-
765 Chem/R2D-VBS simulations; YL, RC, and JJ collected the observational data. JS, BZ,
766 and SW analyzed the data; RC, DG, JJ, YG, MS, BC, and HH presented important
767 suggestions for the paper; JS, BZ, and SW wrote the paper with input from all co-
768 authors.

769

770 **Competing interests.** At least one of the (co-)authors is a member of the editorial board
771 of Atmospheric Chemistry and Physics.

772

773 **Acknowledgements.** This study was supported by the National Natural Science
774 Foundation of China (22188102 and 42275110) and Samsung PM_{2.5} SRP.

775

776 **Financial support.** Financial support from National Natural Science Foundation of
777 China (22188102 and 42275110) and Samsung PM_{2.5} SRP.

778 **REFERENCES**

- 779 Almeida, J., Schobesberger, S., Kurten, A., Ortega, I. K., Kupiainen-Maatta, O.,
780 Praplan, A. P., Adamov, A., Amorim, A., Bianchi, F., Breitenlechner, M.,
781 David, A., Dommen, J., Donahue, N. M., Downard, A., Dunne, E., Duplissy,
782 J., Ehrhart, S., Flagan, R. C., Franchin, A., Guida, R., Hakala, J., Hansel, A.,
783 Heinritzi, M., Henschel, H., Jokinen, T., Junninen, H., Kajos, M.,
784 Kangasluoma, J., Keskinen, H., Kupc, A., Kurten, T., Kvashin, A. N.,
785 Laaksonen, A., Lehtipalo, K., Leiminger, M., Leppa, J., Loukonen, V.,
786 Makhmutov, V., Mathot, S., McGrath, M. J., Nieminen, T., Olenius, T.,
787 Onnela, A., Petaja, T., Riccobono, F., Riipinen, I., Rissanen, M., Rondo, L.,
788 Ruuskanen, T., Santos, F. D., Sarnela, N., Schallhart, S., Schnitzhofer, R.,
789 Seinfeld, J. H., Simon, M., Sipila, M., Stozhkov, Y., Stratmann, F., Tome, A.,
790 Trostl, J., Tsagkogeorgas, G., Vaattovaara, P., Viisanen, Y., Virtanen, A., Vrtala,
791 A., Wagner, P. E., Weingartner, E., Wex, H., Williamson, C., Wimmer, D., Ye,
792 P., Yli-Juuti, T., Carslaw, K. S., Kulmala, M., Curtius, J., Baltensperger, U.,
793 Worsnop, D. R., Vehkamäki, H., and Kirkby, J.: Molecular understanding of
794 sulphuric acid-amine particle nucleation in the atmosphere, *Nature*, 502, 359-
795 363, 10.1038/nature12663, 2013.
- 796 Baranzadeh, E., Murphy, B. N., Julin, J., Falahat, S., Reddington, C. L., Arola, A.,
797 Ahlm, L., Mikkonen, S., Fountoukis, C., Patoulias, D., Minikin, A.,
798 Hamburger, T., Laaksonen, A., Pandis, S. N., Vehkamäki, H., Lehtinen, K. E.
799 J., and Riipinen, I.: Implementation of state-of-the-art ternary new-particle
800 formation scheme to the regional chemical transport model PMCAMx-UF in
801 Europe, *Geoscientific Model Development*, 9, 2741-2754, 10.5194/gmd-9-
802 2741-2016, 2016.
- 803 Bergman, T., Laaksonen, A., Korhonen, H., Malila, J., Dunne, E. M., Mielonen, T.,
804 Lehtinen, K. E. J., Kühn, T., Arola, A., and Kokkola, H.: Geographical and
805 diurnal features of amine - enhanced boundary layer nucleation, *Journal of*
806 *Geophysical Research: Atmospheres*, 120, 9606-9624, 10.1002/2015jd023181,
807 2015.
- 808 Besel, V., Kubecka, J., Kurten, T., and Vehkamäki, H.: Impact of Quantum Chemistry
809 Parameter Choices and Cluster Distribution Model Settings on Modeled
810 Atmospheric Particle Formation Rates, *J Phys Chem A*, 124, 5931-5943,
811 10.1021/acs.jpca.0c03984, 2020.
- 812 Brasseur GP, Jacob DJ. Model Equations and Numerical Approaches. In: *Modeling of*
813 *Atmospheric Chemistry*. Cambridge University Press; 2017:84-204.
- 814 Cai, R. and Jiang, J.: A new balance formula to estimate new particle formation rate:
815 reevaluating the effect of coagulation scavenging, *Atmospheric Chemistry and*
816 *Physics*, 17, 12659-12675, 10.5194/acp-17-12659-2017, 2017.
- 817 Cai, R., Yin, R., Li, X., Xie, H.-B., Yang, D., Kerminen, V.-M., Smith, J. N., Ma, Y.,
818 Hao, J., Chen, J., Kulmala, M., Zheng, J., Jiang, J., and Elm, J.: Significant
819 contributions of trimethylamine to sulfuric acid nucleation in polluted

820 environments, *npj Climate and Atmospheric Science*, 6, 10.1038/s41612-023-
821 00405-3, 2023.

822 Cai, R., Yan, C., Yang, D., Yin, R., Lu, Y., Deng, C., Fu, Y., Ruan, J., Li, X.,
823 Kontkanen, J., Zhang, Q., Kangasluoma, J., Ma, Y., Hao, J., Worsnop, D. R.,
824 Bianchi, F., Paasonen, P., Kerminen, V.-M., Liu, Y., Wang, L., Zheng, J.,
825 Kulmala, M., and Jiang, J.: Sulfuric acid–amine nucleation in urban Beijing,
826 *Atmospheric Chemistry and Physics*, 21, 2457-2468, 10.5194/acp-21-2457-
827 2021, 2021.

828 Chu, B., Kerminen, V.-M., Bianchi, F., Yan, C., Petäjä, T., and Kulmala, M.:
829 Atmospheric new particle formation in China, *Atmospheric Chemistry and*
830 *Physics*, 19, 115-138, 10.5194/acp-19-115-2019, 2019.

831 Croft, B., Wentworth, G. R., Martin, R. V., Leaitch, W. R., Murphy, J. G., Murphy, B.
832 N., Kodros, J. K., Abbatt, J. P. D., and Pierce, J. R.: Contribution of Arctic
833 seabird-colony ammonia to atmospheric particles and cloud-albedo radiative
834 effect, *Nature Communications*, 7, 10.1038/ncomms13444, 2016.

835 Dal Maso, M., Hyvärinen, A., Komppula, M., Tunved, P., Kerminen, V.-M.,
836 Lihavainen, H., Viisanen, Y., Hansson, H.-C., and Kulmala, M.: Annual and
837 interannual variation in boreal forest aerosol particle number and volume
838 concentration and their connection to particle formation, *Tellus B: Chemical*
839 *and Physical Meteorology*, 60, 10.1111/j.1600-0889.2008.00366.x, 2008.

840 Deng, C., Fu, Y., Dada, L., Yan, C., Cai, R., Yang, D., Zhou, Y., Yin, R., Lu, Y., Li, X.,
841 Qiao, X., Fan, X., Nie, W., Kontkanen, J., Kangasluoma, J., Chu, B., Ding, A.,
842 Kerminen, V. M., Paasonen, P., Worsnop, D. R., Bianchi, F., Liu, Y., Zheng, J.,
843 Wang, L., Kulmala, M., and Jiang, J.: Seasonal Characteristics of New Particle
844 Formation and Growth in Urban Beijing, *Environ Sci Technol*, 54, 8547-8557,
845 10.1021/acs.est.0c00808, 2020.

846 Dunne, E. M., Gordon, H., Kurten, A., Almeida, J., Duplissy, J., Williamson, C.,
847 Ortega, I. K., Pringle, K. J., Adamov, A., Baltensperger, U., Barmet, P.,
848 Benduhn, F., Bianchi, F., Breitenlechner, M., Clarke, A., Curtius, J., Dommen,
849 J., Donahue, N. M., Ehrhart, S., Flagan, R. C., Franchin, A., Guida, R.,
850 Hakala, J., Hansel, A., Heinritzi, M., Jokinen, T., Kangasluoma, J., Kirkby, J.,
851 Kulmala, M., Kupc, A., Lawler, M. J., Lehtipalo, K., Makhmutov, V., Mann,
852 G., Mathot, S., Merikanto, J., Miettinen, P., Nenes, A., Onnela, A., Rap, A.,
853 Reddington, C. L., Riccobono, F., Richards, N. A., Rissanen, M. P., Rondo, L.,
854 Sarnela, N., Schobesberger, S., Sengupta, K., Simon, M., Sipila, M., Smith, J.
855 N., Stozkhov, Y., Tome, A., Trostl, J., Wagner, P. E., Wimmer, D., Winkler, P.
856 M., Worsnop, D. R., and Carslaw, K. S.: Global atmospheric particle
857 formation from CERN CLOUD measurements, *Science*, 354, 1119-1124,
858 10.1126/science.aaf2649, 2016.

859 Elm, J., Bilde, M., and Mikkelsen, K. V.: Assessment of binding energies of
860 atmospherically relevant clusters, *Phys Chem Chem Phys*, 15, 16442-16445,
861 10.1039/c3cp52616j, 2013.

862 Elm, J., Kubečka, J., Besel, V., Jääskeläinen, M. J., Halonen, R., Kurtén, T., and
863 Vehkamäki, H.: Modeling the formation and growth of atmospheric molecular
864 clusters: A review, *Journal of Aerosol Science*, 149,
865 10.1016/j.jaerosci.2020.105621, 2020.

866 Gao, D., Zhao, B., Wang, S. X., Shen, J. W., Wang, Y., Zhou, C., Jiang, J. K., Wu, Q.
867 R., Li, S. Y., Sun, Y. S., He, Y. C., Zhu, Y., and Jiang, Z.: Distinct PM_{2.5}-
868 Related Near-Term Climate Penalties Induced by Different Clean Air
869 Measures in China, *Geophysical Research Letters*, 51, 10.1029/2024gl1108204,
870 2024.

871 Gordon, H., Sengupta, K., Rap, A., Duplissy, J., Frege, C., Williamson, C., Heinritzi,
872 M., Simon, M., Yan, C., Almeida, J., Trostl, J., Nieminen, T., Ortega, I. K.,
873 Wagner, R., Dunne, E. M., Adamov, A., Amorim, A., Bernhammer, A. K.,
874 Bianchi, F., Breitenlechner, M., Brilke, S., Chen, X., Craven, J. S., Dias, A.,
875 Ehrhart, S., Fischer, L., Flagan, R. C., Franchin, A., Fuchs, C., Guida, R.,
876 Hakala, J., Hoyle, C. R., Jokinen, T., Junninen, H., Kangasluoma, J., Kim, J.,
877 Kirkby, J., Krapf, M., Kurten, A., Laaksonen, A., Lehtipalo, K., Makhmutov,
878 V., Mathot, S., Molteni, U., Monks, S. A., Onnela, A., Perakyla, O., Piel, F.,
879 Petaja, T., Praplan, A. P., Pringle, K. J., Richards, N. A., Rissanen, M. P.,
880 Rondo, L., Sarnela, N., Schobesberger, S., Scott, C. E., Seinfeld, J. H.,
881 Sharma, S., Sipila, M., Steiner, G., Stozhkov, Y., Stratmann, F., Tome, A.,
882 Virtanen, A., Vogel, A. L., Wagner, A. C., Wagner, P. E., Weingartner, E.,
883 Wimmer, D., Winkler, P. M., Ye, P., Zhang, X., Hansel, A., Dommen, J.,
884 Donahue, N. M., Worsnop, D. R., Baltensperger, U., Kulmala, M., Curtius, J.,
885 and Carslaw, K. S.: Reduced anthropogenic aerosol radiative forcing caused
886 by biogenic new particle formation, *Proc Natl Acad Sci U S A*, 113, 12053-
887 12058, 10.1073/pnas.1602360113, 2016.

888 Guenther, A., Karl, T., Harley, P., Wiedinmyer, C., Palmer, P. I., and Geron, C.:
889 Estimates of global terrestrial isoprene emissions using MEGAN (Model of
890 Emissions of Gases and Aerosols from Nature), *Atmos. Chem. Phys.*, 6, 3181-
891 3210, 10.5194/acp-6-3181-2006, 2006.

892 He, X. C., Tham, Y. J., Dada, L., Wang, M., Finkenzeller, H., Stolzenburg, D., Iyer, S.,
893 Simon, M., Kurten, A., Shen, J., Rorup, B., Rissanen, M., Schobesberger, S.,
894 Baalbaki, R., Wang, D. S., Koenig, T. K., Jokinen, T., Sarnela, N., Beck, L. J.,
895 Almeida, J., Amanatidis, S., Amorim, A., Ataei, F., Baccarini, A., Bertozzi, B.,
896 Bianchi, F., Brilke, S., Caudillo, L., Chen, D., Chiu, R., Chu, B., Dias, A.,
897 Ding, A., Dommen, J., Duplissy, J., El Haddad, I., Gonzalez Carracedo, L.,
898 Granzin, M., Hansel, A., Heinritzi, M., Hofbauer, V., Junninen, H.,
899 Kangasluoma, J., Kempainen, D., Kim, C., Kong, W., Krechmer, J. E.,
900 Kvashin, A., Laitinen, T., Lamkaddam, H., Lee, C. P., Lehtipalo, K.,
901 Leiminger, M., Li, Z., Makhmutov, V., Manninen, H. E., Marie, G., Marten,
902 R., Mathot, S., Mauldin, R. L., Mentler, B., Mohler, O., Muller, T., Nie, W.,
903 Onnela, A., Petaja, T., Pfeifer, J., Philippov, M., Ranjithkumar, A., Saiz-Lopez,

904 A., Salma, I., Scholz, W., Schuchmann, S., Schulze, B., Steiner, G., Stozhkov,
 905 Y., Tauber, C., Tome, A., Thakur, R. C., Vaisanen, O., Vazquez-Pufleau, M.,
 906 Wagner, A. C., Wang, Y., Weber, S. K., Winkler, P. M., Wu, Y., Xiao, M., Yan,
 907 C., Ye, Q., Ylisirnio, A., Zauner-Wieczorek, M., Zha, Q., Zhou, P., Flagan, R.
 908 C., Curtius, J., Baltensperger, U., Kulmala, M., Kerminen, V. M., Kurten, T.,
 909 Donahue, N. M., Volkamer, R., Kirkby, J., Worsnop, D. R., and Sipila, M.:
 910 Role of iodine oxoacids in atmospheric aerosol nucleation, *Science*, 371, 589-
 911 595, 10.1126/science.abe0298, 2021.

912 Jen, C. N., Hanson, D. R., and McMurry, P. H.: Toward Reconciling Measurements of
 913 Atmospherically Relevant Clusters by Chemical Ionization Mass
 914 Spectrometry and Mobility Classification/Vapor Condensation, *Aerosol
 915 Science and Technology*, 49, i-iii, 10.1080/02786826.2014.1002602, 2014.

916 Julin, J., Murphy, B. N., Patoulias, D., Fountoukis, C., Olenius, T., Pandis, S. N., and
 917 Riipinen, I.: Impacts of Future European Emission Reductions on Aerosol
 918 Particle Number Concentrations Accounting for Effects of Ammonia, Amines,
 919 and Organic Species, *Environ Sci Technol*, 52, 692-700,
 920 10.1021/acs.est.7b05122, 2018.

921 Kirkby, J., Curtius, J., Almeida, J., Dunne, E., Duplissy, J., Ehrhart, S., Franchin, A.,
 922 Gagne, S., Ickes, L., Kurten, A., Kupc, A., Metzger, A., Riccobono, F., Rondo,
 923 L., Schobesberger, S., Tsagkogeorgas, G., Wimmer, D., Amorim, A., Bianchi,
 924 F., Breitenlechner, M., David, A., Dommen, J., Downard, A., Ehn, M., Flagan,
 925 R. C., Haider, S., Hansel, A., Hauser, D., Jud, W., Junninen, H., Kreissl, F.,
 926 Kvashin, A., Laaksonen, A., Lehtipalo, K., Lima, J., Lovejoy, E. R.,
 927 Makhmutov, V., Mathot, S., Mikkila, J., Minginette, P., Mogo, S., Nieminen,
 928 T., Onnela, A., Pereira, P., Petaja, T., Schnitzhofer, R., Seinfeld, J. H., Sipila,
 929 M., Stozhkov, Y., Stratmann, F., Tome, A., Vanhanen, J., Viisanen, Y., Vrtala,
 930 A., Wagner, P. E., Walther, H., Weingartner, E., Wex, H., Winkler, P. M.,
 931 Carslaw, K. S., Worsnop, D. R., Baltensperger, U., and Kulmala, M.: Role of
 932 sulphuric acid, ammonia and galactic cosmic rays in atmospheric aerosol
 933 nucleation, *Nature*, 476, 429-433, 10.1038/nature10343, 2011.

934 Kirkby, J., Duplissy, J., Sengupta, K., Frege, C., Gordon, H., Williamson, C.,
 935 Heinritzi, M., Simon, M., Yan, C., Almeida, J., Trostl, J., Nieminen, T., Ortega,
 936 I. K., Wagner, R., Adamov, A., Amorim, A., Bernhammer, A. K., Bianchi, F.,
 937 Breitenlechner, M., Brilke, S., Chen, X., Craven, J., Dias, A., Ehrhart, S.,
 938 Flagan, R. C., Franchin, A., Fuchs, C., Guida, R., Hakala, J., Hoyle, C. R.,
 939 Jokinen, T., Junninen, H., Kangasluoma, J., Kim, J., Krapf, M., Kurten, A.,
 940 Laaksonen, A., Lehtipalo, K., Makhmutov, V., Mathot, S., Molteni, U.,
 941 Onnela, A., Perakyla, O., Piel, F., Petaja, T., Praplan, A. P., Pringle, K., Rap,
 942 A., Richards, N. A., Riipinen, I., Rissanen, M. P., Rondo, L., Sarnela, N.,
 943 Schobesberger, S., Scott, C. E., Seinfeld, J. H., Sipila, M., Steiner, G.,
 944 Stozhkov, Y., Stratmann, F., Tome, A., Virtanen, A., Vogel, A. L., Wagner, A.
 945 C., Wagner, P. E., Weingartner, E., Wimmer, D., Winkler, P. M., Ye, P., Zhang,

946 X., Hansel, A., Dommen, J., Donahue, N. M., Worsnop, D. R., Baltensperger,
947 U., Kulmala, M., Carslaw, K. S., and Curtius, J.: Ion-induced nucleation of
948 pure biogenic particles, *Nature*, 533, 521-526, 10.1038/nature17953, 2016.

949 Kulmala, M., Lehtinen, K. E. J., and Laaksonen, A.: Cluster activation theory as an
950 explanation of the linear dependence between formation rate of 3nm particles
951 and sulphuric acid concentration, *Atmospheric Chemistry and Physics*, 6, 787-
952 793, DOI 10.5194/acp-6-787-2006, 2006.

953 Kürten, A., Li, C., Bianchi, F., Curtius, J., Dias, A., Donahue, N. M., Duplissy, J.,
954 Flagan, R. C., Hakala, J., Jokinen, T., Kirkby, J., Kulmala, M., Laaksonen, A.,
955 Lehtipalo, K., Makhmutov, V., Onnela, A., Rissanen, M. P., Simon, M., Sipilä,
956 M., Stozhkov, Y., Tröstl, J., Ye, P., and McMurry, P. H.: New particle
957 formation in the sulfuric acid–dimethylamine–water system: reevaluation of
958 CLOUD chamber measurements and comparison to an aerosol nucleation and
959 growth model, *Atmospheric Chemistry and Physics*, 18, 845-863,
960 10.5194/acp-18-845-2018, 2018.

961 Lehtinen, K. E. J., Dal Maso, M., Kulmala, M., and Kerminen, V. M.: Estimating
962 nucleation rates from apparent particle formation rates and vice versa: Revised
963 formulation of the Kerminen-Kulmala equation, *Journal of Aerosol Science*,
964 38, 988-994, 10.1016/j.jaerosci.2007.06.009, 2007.

965 Li, C., Zhao, Y., Li, Z., Liu, L., Zhang, X., Zheng, J., Kerminen, V.-M., Kulmala, M.,
966 Jiang, J., Cai, R., and Xiao, H.: The dependence of new particle formation
967 rates on the interaction between cluster growth, evaporation, and condensation
968 sink, *Environmental Science: Atmospheres*, 3, 168-181, 10.1039/d2ea00066k,
969 2023a.

970 Li, H., Ning, A., Zhong, J., Zhang, H., Liu, L., Zhang, Y., Zhang, X., Zeng, X. C., and
971 He, H.: Influence of atmospheric conditions on sulfuric acid-dimethylamine-
972 ammonia-based new particle formation, *Chemosphere*, 245, 125554,
973 10.1016/j.chemosphere.2019.125554, 2020.

974 Li, M., Zhang, Q., Kurokawa, J., Woo, J. H., He, K. B., Lu, Z. F., Ohara, T., Song, Y.,
975 Streets, D. G., Carmichael, G. R., Cheng, Y. F., Hong, C. P., Huo, H., Jiang, X.
976 J., Kang, S. C., Liu, F., Su, H., and Zheng, B.: MIX: a mosaic Asian
977 anthropogenic emission inventory under the international collaboration
978 framework of the MICS-Asia and HTAP, *Atmospheric Chemistry and Physics*,
979 17, 935-963, 10.5194/acp-17-935-2017, 2017.

980 Li, S., Wang, S., Wu, Q., Zhang, Y., Ouyang, D., Zheng, H., Han, L., Qiu, X., Wen, Y.,
981 Liu, M., Jiang, Y., Yin, D., Liu, K., Zhao, B., Zhang, S., Wu, Y., and Hao, J.:
982 Emission trends of air pollutants and CO₂ in China from 2005 to 2021, *Earth
983 System Science Data*, 15, 2279-2294, 10.5194/essd-15-2279-2023, 2023b.

984 Li, Y., Shen, J., Zhao, B., Cai, R., Wang, S., Gao, Y., Shrivastava, M., Gao, D., Zheng,
985 J., Kulmala, M., and Jiang, J.: A dynamic parameterization of sulfuric acid–
986 dimethylamine nucleation and its application in three-dimensional modeling,
987 *Atmospheric Chemistry and Physics*, 23, 8789-8804, 10.5194/acp-23-8789-

988 2023, 2023c.

989 Liu, L., Yu, F., Tu, K., Yang, Z., and Zhang, X.: Influence of atmospheric conditions
990 on the role of trifluoroacetic acid in atmospheric sulfuric acid–dimethylamine
991 nucleation, *Atmospheric Chemistry and Physics*, 21, 6221-6230, 10.5194/acp-
992 21-6221-2021, 2021.

993 Liu, L., Zhong, J., Vehkamäki, H., Kurtén, T., Du, L., Zhang, X., Francisco, J. S., and
994 Zeng, X. C.: Unexpected quenching effect on new particle formation from the
995 atmospheric reaction of methanol with SO₃, *Proc Natl Acad Sci U S A*, 116,
996 24966-24971, 10.1073/pnas.1915459116, 2019.

997 Lu, Y., Liu, L., Ning, A., Yang, G., Liu, Y., Kurtén, T., Vehkamäki, H., Zhang, X., and
998 Wang, L.: Atmospheric Sulfuric Acid - Dimethylamine Nucleation Enhanced
999 by Trifluoroacetic Acid, *Geophysical Research Letters*, 47,
1000 10.1029/2019gl085627, 2020.

1001 Ma, F., Xie, H. B., Elm, J., Shen, J., Chen, J., and Vehkamäki, H.: Piperazine
1002 Enhancing Sulfuric Acid-Based New Particle Formation: Implications for the
1003 Atmospheric Fate of Piperazine, *Environ Sci Technol*, 53, 8785-8795,
1004 10.1021/acs.est.9b02117, 2019.

1005 McGrath, M. J., Olenius, T., Ortega, I. K., Loukonen, V., Paasonen, P., Kurtén, T.,
1006 Kulmala, M., and Vehkamäki, H.: Atmospheric Cluster Dynamics Code: a
1007 flexible method for solution of the birth-death equations, *Atmospheric
1008 Chemistry and Physics*, 12, 2345-2355, 10.5194/acp-12-2345-2012, 2012.

1009 Myllys, N., Chee, S., Olenius, T., Lawler, M., and Smith, J.: Molecular-Level
1010 Understanding of Synergistic Effects in Sulfuric Acid-Amine-Ammonia
1011 Mixed Clusters, *J Phys Chem A*, 123, 2420-2425, 10.1021/acs.jpca.9b00909,
1012 2019.

1013 Ning, A. and Zhang, X.: The synergistic effects of methanesulfonic acid (MSA) and
1014 methanesulfinic acid (MSIA) on marine new particle formation, *Atmospheric
1015 Environment*, 269, 10.1016/j.atmosenv.2021.118826, 2022.

1016 Ning, A., Liu, L., Ji, L., and Zhang, X.: Molecular-level nucleation mechanism of
1017 iodic acid and methanesulfonic acid, *Atmospheric Chemistry and Physics*, 22,
1018 6103-6114, 10.5194/acp-22-6103-2022, 2022.

1019 Ning, A., Zhang, H., Zhang, X., Li, Z., Zhang, Y., Xu, Y., and Ge, M.: A molecular-
1020 scale study on the role of methanesulfinic acid in marine new particle
1021 formation, *Atmospheric Environment*, 227, 10.1016/j.atmosenv.2020.117378,
1022 2020.

1023 Ning, A., Shen, J., Zhao, B., Wang, S., Cai, R., Jiang, J. Yan, C., Fu, X., Zhang, Y., Li,
1024 J., Ouyang, D., Sun, Y., Saiz-Lopez, A., Francisco, J., and Zhang, X.:
1025 Overlooked significance of iodic acid in new particle formation in the
1026 continental atmosphere, *Proc Natl Acad Sci U S A*, 2024. 121 (31),
1027 e2404595121.

1028 Olenius, T., Kupiainen-Maatta, O., Ortega, I. K., Kurtén, T., and Vehkamäki, H.: Free
1029 energy barrier in the growth of sulfuric acid-ammonia and sulfuric acid-

1030 dimethylamine clusters, *J Chem Phys*, 139, 084312, 10.1063/1.4819024, 2013.

1031 Olenius, T., Halonen, R., Kurtén, T., Henschel, H., Kupiainen - Määttä, O., Ortega, I.

1032 K., Jen, C. N., Vehkamäki, H., and Riipinen, I.: New particle formation from

1033 sulfuric acid and amines: Comparison of monomethylamine, dimethylamine,

1034 and trimethylamine, *Journal of Geophysical Research: Atmospheres*, 122,

1035 7103-7118, 10.1002/2017jd026501, 2017.

1036 Olenius, T. and Roldin, P.: Role of gas-molecular cluster-aerosol dynamics in

1037 atmospheric new-particle formation, *Sci Rep*, 12, 10135, 10.1038/s41598-022-

1038 14525-y, 2022.

1039 Olin, M., Patoulias, D., Kuuluvainen, H., Niemi, J. V., Rönkkö, T., Pandis, S. N.,

1040 Riipinen, I., and Dal Maso, M.: Contribution of traffic-originated nanoparticle

1041 emissions to regional and local aerosol levels, *Atmospheric Chemistry and*

1042 *Physics*, 22, 1131-1148, 10.5194/acp-22-1131-2022, 2022.

1043 Ortega, I. K., Kupiainen, O., Kurtén, T., Olenius, T., Wilkman, O., McGrath, M. J.,

1044 Loukonen, V., and Vehkamäki, H.: From quantum chemical formation free

1045 energies to evaporation rates, *Atmospheric Chemistry and Physics*, 12, 225-

1046 235, 10.5194/acp-12-225-2012, 2012.

1047 Riccobono, F., Schobesberger, S., Scott, C. E., Dommen, J., Ortega, I. K., Rondo, L.,

1048 Almeida, J., Amorim, A., Bianchi, F., Breitenlechner, M., David, A., Downard,

1049 A., Dunne, E. M., Duplissy, J., Ehrhart, S., Flagan, R. C., Franchin, A.,

1050 Hansel, A., Junninen, H., Kajos, M., Keskinen, H., Kupc, A., Kurten, A.,

1051 Kvashin, A. N., Laaksonen, A., Lehtipalo, K., Makhmutov, V., Mathot, S.,

1052 Nieminen, T., Onnela, A., Petaja, T., Praplan, A. P., Santos, F. D., Schallhart,

1053 S., Seinfeld, J. H., Sipila, M., Spracklen, D. V., Stozhkov, Y., Stratmann, F.,

1054 Tome, A., Tsagkogeorgas, G., Vaattovaara, P., Viisanen, Y., Vrtala, A., Wagner,

1055 P. E., Weingartner, E., Wex, H., Wimmer, D., Carslaw, K. S., Curtius, J.,

1056 Donahue, N. M., Kirkby, J., Kulmala, M., Worsnop, D. R., and Baltensperger,

1057 U.: Oxidation Products of Biogenic Emissions Contribute to Nucleation of

1058 Atmospheric Particles, *Science*, 344, 717-721, 10.1126/science.1243527,

1059 2014.

1060 Semeniuk, K. and Dastoor, A.: Current state of aerosol nucleation parameterizations

1061 for air-quality and climate modeling, *Atmospheric Environment*, 179, 77-106,

1062 10.1016/j.atmosenv.2018.01.039, 2018.

1063 Stolzenburg, D., Simon, M., Ranjithkumar, A., Kürten, A., Lehtipalo, K., Gordon, H.,

1064 Ehrhart, S., Finkenzeller, H., Pichelstorfer, L., Nieminen, T., He, X.-C., Brilke,

1065 S., Xiao, M., Amorim, A., Baalbaki, R., Baccarini, A., Beck, L., Bräkling, S.,

1066 Caudillo Murillo, L., Chen, D., Chu, B., Dada, L., Dias, A., Dommen, J.,

1067 Duplissy, J., El Haddad, I., Fischer, L., Gonzalez Carracedo, L., Heinritzi, M.,

1068 Kim, C., Koenig, T. K., Kong, W., Lamkaddam, H., Lee, C. P., Leiminger, M.,

1069 Li, Z., Makhmutov, V., Manninen, H. E., Marie, G., Marten, R., Müller, T.,

1070 Nie, W., Partoll, E., Petäjä, T., Pfeifer, J., Philippov, M., Rissanen, M. P.,

1071 Rörup, B., Schobesberger, S., Schuchmann, S., Shen, J., Sipilä, M., Steiner,

1072 G., Stozhkov, Y., Tauber, C., Tham, Y. J., Tomé, A., Vazquez-Pufleau, M.,
1073 Wagner, A. C., Wang, M., Wang, Y., Weber, S. K., Wimmer, D., Wlasits, P. J.,
1074 Wu, Y., Ye, Q., Zauner-Wieczorek, M., Baltensperger, U., Carslaw, K. S.,
1075 Curtius, J., Donahue, N. M., Flagan, R. C., Hansel, A., Kulmala, M.,
1076 Lelieveld, J., Volkamer, R., Kirkby, J., and Winkler, P. M.: Enhanced growth
1077 rate of atmospheric particles from sulfuric acid, *Atmospheric Chemistry and*
1078 *Physics*, 20, 7359-7372, 10.5194/acp-20-7359-2020, 2020.

1079 Svenhag, C., Sporre, M. K., Olenius, T., Yazgi, D., Blichner, S. M., Nieradzick, L. P.,
1080 and Roldin, P.: Implementing detailed nucleation predictions in the Earth
1081 system model EC-Earth3.3.4: sulfuric acid-ammonia nucleation, *EGUsphere*
1082 [preprint], <https://doi.org/10.5194/egusphere-2023-2665>, 2024.

1083 Thomas, J. M., He, S., Larriba-Andaluz, C., DePalma, J. W., Johnston, M. V., and
1084 Hogan, C. J., Jr.: Ion mobility spectrometry-mass spectrometry examination of
1085 the structures, stabilities, and extents of hydration of dimethylamine-sulfuric
1086 acid clusters, *Phys Chem Chem Phys*, 18, 22962-22972, 10.1039/c6cp03432b,
1087 2016.

1088 Xiao, M., Hoyle, C. R., Dada, L., Stolzenburg, D., Kürten, A., Wang, M.,
1089 Lamkaddam, H., Garmash, O., Mentler, B., Molteni, U., Baccharini, A., Simon,
1090 M., He, X.-C., Lehtipalo, K., Ahonen, L. R., Baalbaki, R., Bauer, P. S., Beck,
1091 L., Bell, D., Bianchi, F., Brilke, S., Chen, D., Chiu, R., Dias, A., Duplissy, J.,
1092 Finkenzeller, H., Gordon, H., Hofbauer, V., Kim, C., Koenig, T. K.,
1093 Lampilahti, J., Lee, C. P., Li, Z., Mai, H., Makhmutov, V., Manninen, H. E.,
1094 Marten, R., Mathot, S., Mauldin, R. L., Nie, W., Onnela, A., Partoll, E., Petäjä,
1095 T., Pfeifer, J., Pospisilova, V., Quéléver, L. L. J., Rissanen, M., Schobesberger,
1096 S., Schuchmann, S., Stozhkov, Y., Tauber, C., Tham, Y. J., Tomé, A., Vazquez-
1097 Pufleau, M., Wagner, A. C., Wagner, R., Wang, Y., Weitz, L., Wimmer, D., Wu,
1098 Y., Yan, C., Ye, P., Ye, Q., Zha, Q., Zhou, X., Amorim, A., Carslaw, K.,
1099 Curtius, J., Hansel, A., Volkamer, R., Winkler, P. M., Flagan, R. C., Kulmala,
1100 M., Worsnop, D. R., Kirkby, J., Donahue, N. M., Baltensperger, U., El
1101 Haddad, I., and Dommen, J.: The driving factors of new particle formation and
1102 growth in the polluted boundary layer, *Atmospheric Chemistry and Physics*,
1103 21, 14275-14291, 10.5194/acp-21-14275-2021, 2021.

1104 Xie, H. B., Elm, J., Halonen, R., Myllys, N., Kurten, T., Kulmala, M., and Vehkamäki,
1105 H.: Atmospheric Fate of Monoethanolamine: Enhancing New Particle
1106 Formation of Sulfuric Acid as an Important Removal Process, *Environ Sci*
1107 *Technol*, 51, 8422-8431, 10.1021/acs.est.7b02294, 2017.

1108 Yang, S., Liu, Z., Clusius, P. S., Liu, Y., Zou, J., Yang, Y., Zhao, S., Zhang, G., Xu, Z.,
1109 Ma, Z., Yang, Y., Sun, J., Pan, Y., Ji, D., Hu, B., Yan, C., Boy, M., Kulmala,
1110 M., and Wang, Y.: Chemistry of new particle formation and growth events
1111 during wintertime in suburban area of Beijing: Insights from highly polluted
1112 atmosphere, *Atmospheric Research*, 255, 10.1016/j.atmosres.2021.105553,
1113 2021.

1114 Yao, L., Garmash, O., Bianchi, F., Zheng, J., Yan, C., Kontkanen, J., Junninen, H.,
1115 Mazon, S. B., Ehn, M., Paasonen, P., Sipila, M., Wang, M., Wang, X., Xiao,
1116 S., Chen, H., Lu, Y., Zhang, B., Wang, D., Fu, Q., Geng, F., Li, L., Wang, H.,
1117 Qiao, L., Yang, X., Chen, J., Kerminen, V. M., Petaja, T., Worsnop, D. R.,
1118 Kulmala, M., and Wang, L.: Atmospheric new particle formation from sulfuric
1119 acid and amines in a Chinese megacity, *Science*, 361, 278-281,
1120 10.1126/science.aao4839, 2018.

1121 Yazgi, D. and Olenius, T.: J-GAIN v1.1: a flexible tool to incorporate aerosol
1122 formation rates obtained by molecular models into large-scale models,
1123 *Geoscientific Model Development*, 16, 5237-5249, 10.5194/gmd-16-5237-
1124 2023, 2023.

1125 Yu, F.: Ion-mediated nucleation in the atmosphere: Key controlling parameters,
1126 implications, and look-up table, *Journal of Geophysical Research*, 115,
1127 10.1029/2009jd012630, 2010.

1128 Zhao, B., Shrivastava, M., Donahue, N. M., Gordon, H., Schervish, M., Shilling, J. E.,
1129 Zaveri, R. A., Wang, J., Andreae, M. O., Zhao, C., Gaudet, B., Liu, Y., Fan, J.,
1130 and Fast, J. D.: High concentration of ultrafine particles in the Amazon free
1131 troposphere produced by organic new particle formation, *Proc Natl Acad Sci*
1132 *U S A*, 117, 25344-25351, 10.1073/pnas.2006716117, 2020.

1133 Zheng, H. T., Cai, S. Y., Wang, S. X., Zhao, B., Chang, X., and Hao, J. M.:
1134 Development of a unit-based industrial emission inventory in the Beijing-
1135 Tianjin-Hebei region and resulting improvement in air quality modeling,
1136 *Atmospheric Chemistry and Physics*, 19, 3447-3462, 10.5194/acp-19-3447-
1137 2019, 2019.

1138 Zhu, S., Yan, C., Zheng, J., Chen, C., Ning, H., Yang, D., Wang, M., Ma, Y., Zhan, J.,
1139 Hua, C., Yin, R., Li, Y., Liu, Y., Jiang, J., Yao, L., Wang, L., Kulmala, M., and
1140 Worsnop, D. R.: Observation and Source Apportionment of Atmospheric
1141 Alkaline Gases in Urban Beijing, *Environ Sci Technol*, 56, 17545-17555,
1142 10.1021/acs.est.2c03584, 2022.